12-2010

ULTRAFAST TIME DOMAIN OPTICS OF SINGLE-CYCLE LASER PULSE INTERACTION WITH MATERIALS

Ufuk Parali
University of Nebraska - Lincoln, ufukparali@yahoo.com

ULTRAFAST TIME DOMAIN OPTICS OF SINGLE-CYCLE LASER PULSE INTERACTION WITH MATERIALS

by

Ufuk Parali

A DISSERTATION

Presented to the Faculty of

The Graduate College at the University of Nebraska

In Partial Fulfillment of Requirements

For the Degree of Doctor of Philosophy

Major: Engineering
(Electrical Engineering)

Under the Supervision of Professor Dennis R. Alexander

Lincoln, Nebraska

December, 2010

ULTRAFAST TIME DOMAIN OPTICS OF SINGLE-CYCLE LASER PULSE INTERACTION WITH MATERIALS

Ufuk Parali, Ph.D.

University of Nebraska, 2010

Advisor: Dennis R. Alexander

In this thesis, interaction of an ultrashort single-cycle pulse (USCP) with a bound electron without ionization is studied for the first time. For a more realistic mathematical description of USCPs, Hermitian polynomials and combination of Laguerre functions are used for two different single-cycle excitation cases. These single-cycle pulse models are used as driving functions for the classical approach to model the interaction of a bound electron with an applied field. Two different new novel time domain modification techniques are developed for modifying the classical Lorentz damped oscillator model in order to make it compatible with the USCP excitation. In the first technique, a time dependent modifier function (MF) approach has been developed that turns the Lorentz oscillator model equation into a Hill-like equation with non-periodic time varying damping and spring coefficients. In the second technique, a time dependent convolutional modifier function (CMF) approach has been developed for a close resonance excitation case. This technique provides a continuous updating of the bound electron motion under USCP excitation with CMF time upgrading of the oscillation motion for the bound electron. We apply each technique with our two different driving model excitations. Each model provides a

quite different time response of the bound electron for the same applied time domain technique. Different polarization response will subsequently result in relative differences in the time dependent index of refraction. We show that the differences in the two types of input oscillation fields cause subduration time regions where the perturbation on the real and imaginary part of the index of refraction dominate successively.

ACKNOWLEDGMENTS

I would like to express my deepest appreciation to all those who have extended their generous help during my Ph.D. program and made this work possible.

The very first person I would be grateful of is my advisor Prof. Dennis R. Alexander for his mentorship and advising throughout my graduate work. He has intrigued me at the beginning of my program to think on some of the fundamentals of ultrashort pulse phenomena and ultrashort single-cycle pulse phenomena. I have always learned something new from Prof. Alexander and over the years I came to appreciate his remarkable guidance and support. Without his expertise and encouragement, this thesis would not have been possible. I would also like to thank my thesis committee members Prof. Yongfeng Lu, Prof. Ezekiel Bahar and Prof. Cornelis J. Uiterwaal for reading and correcting the dissertation. Our long discussions with Prof. Bahar and Prof. Uiterwaal were not only inspirational but also extremely helpful for understanding the theoretical underpinnings of our work. I am thankful for their support and advice in electromagnetics and ultrafast optics.

I would like to thank to my friends in our group for their fellowship and support: Craig Zuhlke, Nicholas Rowse, Ethan Jackson, John Bruce III and Dr. Troy Anderson. I always enjoyed our discussions and I truly appreciate their generosity and friendship. I would also like to thank my friends in different research groups: Tanya Gachovska, Yang Gao, Masoud Mahjouri Samani, Xuejian Li, Arindra Guha and Ufuk Nalbantoglu for their support and great friendship.

I would not have come this far without the love and support of my mother, father, sisters and brothers. Their constant care from a remote distance was the source of my energy for achieving the goal. I cannot express my gratitude for their continuous encouragement and selfless sacrifice. This thesis is dedicated to them.

TABLE OF CONTENTS

NOMENCLATURE

Symbol	Description
w_0	angular frequency
c	speed of light
λ	carrier wavelength
Ω_o	Rabi frequency that produces Stokes sideband
Ω_{-1}	Rabi frequency that produces anti-Stokes sideband
δw	detuning from electronic states
$\lvert\Delta w\rvert$	detuning from Raman sidebands
υ_{ab}	D_2 vibrational transition frequency
T	repetition rate
τ	phase shift
Δt	time delay
m	order of Laguerre function
$L_m(t)$	m^{th} order Laguerre function
z	spatial coordinate on z-axis
t_o	time scale of the pulse
ϕ	initial phase
α	phase term of the electric field
$E(\alpha)$	ultrashort single-cycle electric field

τ_p	pulse duration
n	index of refraction
ε_o	permittivity of free space
μ_o	permeability of free space
$P_{pol}(t)$	electronic polarization
q_e	electron charge
m_e	electron rest mass
$x(t)$	electron oscillation field
$x_o(t)$	modifier function
k_o	spring constant
γ_o	damping constant
$Q(t)$	time dependent spring coefficient
$P(t)$	time dependent damping coefficient
Δw	spectral bandwidth
$f(t)$	trial function for the solution of Volterra Integral Equation
β	phase term of $f(t)$
f_{oi}	coefficient of ith $f(t)$
$x_o'(t)$	1st derivative of the modifier function
$x_o''(t)$	2nd derivative of the modifier function
$x_{oV}(t)$	modifier function found via Volterra Integral Equation solution
$f_V(t)$	$f(t)$ that is found by using $x_{oV}(t)$

CHAPTER 1

INTRODUCTION

The studies on the generation of ultrashort laser pulses that contain only a few cycles of the electric field attracted remarkable attention in the scientific community [1-37]. For the generation of ultrashort pulses, one requires a wide-bandwidth coherent spectrum [2]. An incoherent radiation source, such as sunlight, a high pressure arc lamp or an atomic line emission lamp consists of many spectral components, all with randomly varying phases [2]. The time structure from such a source is white noise [2]. In contrast, a coherent light source has a fixed phase relation among the spectral components, which interfere to produce well-defined waveforms [2]. For more than two decades and until very recently, the shortest optical pulses were obtained by expanding the spectrum of a mode-locked laser by self-phase modulation in an optical fiber, and then compensating for group velocity dispersion by using diffraction grating and prism pairs [3]. Following the report in 1987 of 6 fs optical pulses from a dye laser system [4], ultrashort light pulse research has led to the creation of laser systems generating pulses only a few cycles in duration [4]. Few-cycle transients generation has been boosted by Ti:Sapphire technology [4]. Using sophisticated intracavity dispersion control, a pulse duration of 4.4 fs has been achieved directly with a resonator [4,5]. Ti:Sapphire amplifiers operating at reduced repetition rates enable extreme compression in hollow fibers [4,6,7]. Broadband optical parametric oscillators

[4,8] and amplifiers [4,9] have produced pulses as short as 3.9 fs in the visible [4,10] and 8.5 fs in the near infrared [4,11]. Very recently, 7.8 fs pulses at a central wavelength of 1.2 μm were implemented with erbium-doped fiber technology [4]. All these results correspond to less than two but more than 1.3 oscillation cycles of the electromagnetic field [4]. Since light is an electromagnetic wave, the laser pulses cannot be shorter than the carrier wavelength, λ, which therefore limits the duration of the pulse to λ/c, where c is the speed of light. To synthesize even shorter pulses, the spectra from femtosecond sources may be shaped in amplitude and phase [4,12] or pulse trains at different wavelength may be phase locked and combined [4]. In principle, a sequence of light pulses that are shorter than λ / c can be produced simply by adding together waves [Fig. 1.1] that oscillate with an angular frequency of w_o + MΔw, where Δw is a fixed shift with respect to the fundamental laser wave, $w_o = 2\pi c / \lambda$, and M is an integer [13].

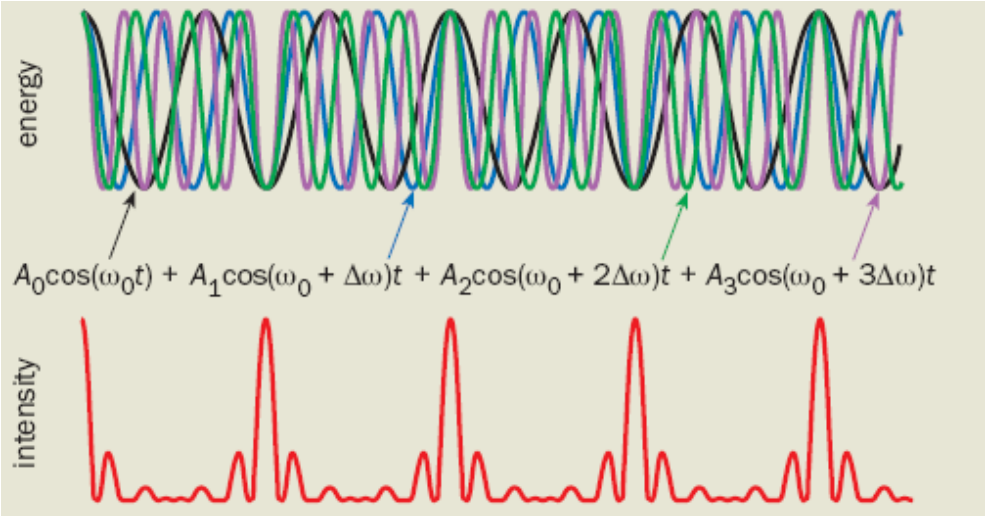

Fig 1.1. How to generate subfemtosecond pulses: The superposition of several light waves at equidistant frequencies (top) in the ultraviolet region can give rise to a sequence of subfemtosecond

spikes (bottom) if the phases of the waves are adjusted appropriately. The repetition rate of the spikes is $\Delta\nu = \Delta w / 2\pi$, where Δw is the angular frequency difference between adjacent components [13].

The result is series of intense spikes separated in time by $1 / \Delta\nu = 2\pi / \Delta w$ [13]. The duration of these spikes is inversely proportional to both the frequency shift, $\Delta\nu$, and the number of waves that add together [13]. Conceptually, this technique is closely related to the mode-locking method that is generally used to generate femtosecond pulses in laser resonators [13]. Indeed, $\Delta\nu$ must be so large that no laser can amplify all these frequency-shifted waves [13]. The only way that these waves can be produced is using nonlinear optical techniques that are not part of the femtosecond laser oscillator itself [13].

For more than a decade, laser physicists and engineers have dreamed of combining the output from two independent mode-locked lasers to synthesize single-cycle pulses through coherent interference [14]. Recently, the studies on the generation of ultrashort laser pulses that contain only a few cycles of the electric field have reached an advanced point where the ultrashort laser pulses contain only a single-cycle of the electric field [2-5,14-24,28-31,33,34]. A single-cycle pulse, the shortest possible waveform at a given wavelength, occurs when the electric field within the envelope of an ultrashort laser pulse performs just one period before the pulse ends [14]. In the infrared region at around 1.5 μm, the duration of one optical cycle is approximately 4 fs [14]. Although the shortest pulses achieved so far have durations of less than 100 attoseconds, they are still multicycle pulses because the frequency of electromagnetic radiation is much higher in the extreme ultraviolet region than the infrared [14].

Today, there are two different approaches to generate single-cycle pulses experimentally. The first approach relies on the adiabatic preparation of highly coherent molecular vibrations or rotations in large ensembles of molecules [3]. The researchers who proposed this approach investigated a broad-band Raman light source, which is based on the collinear generation of wide spectrum of equidistant mutually coherent Raman sidebands [3,26,27]. Raman scattering occurs [Fig. 1.2] when light passes through a gas of molecules [13]. The light can excite vibrational or rotational energy levels in the molecules, which subsequently modulate the laser

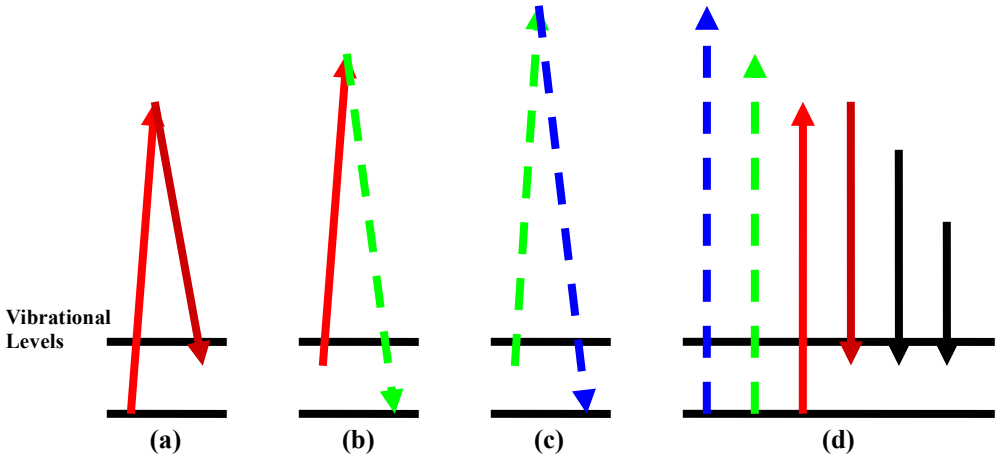

Fig. 1.2. a) The pump (red) and Stokes (dark red) driving lasers drive a molecular vibrational transition slightly off-resonance. b) The pump laser mixes with the molecular vibration to generate an additional anti-Stokes frequency (broken green line). c) The anti-Stokes field mixes with the molecular vibration to generate the next anti-Stokes frequency (broken blue line) d) This process continues to generate both Stokes (solid lines to the right of pump pulse) and anti-Stokes (broken lines to the left of pump pulse). The number of new frequencies depends on the efficiency of the process [2].

radiation [13]. The potential of stimulated Raman scattering for generating trains of subfemtosecond pulses has been demonstrated by several studies [13,24,25,28-34]. In

these studies it has been showed that two laser beams whose frequency difference is slightly offset from a molecular transition will, for an appropriate choice of gas pressure and cell length, generate a spectrum of Raman sidebands whose Fourier transform is a periodic train of subfemtosecond pulses [28]. The essence of the technique [Fig. 1.3] is the concurrent generation of a frequency modulated waveform and the use of group velocity dispersion to temporally compress this waveform [28]. The coherence of the driven molecular transition is central to this technique [28] and it is established by detuning [Fig. 1.3(a)] slightly from the Raman resonance by driving the system with two single-mode laser fields [3,28].

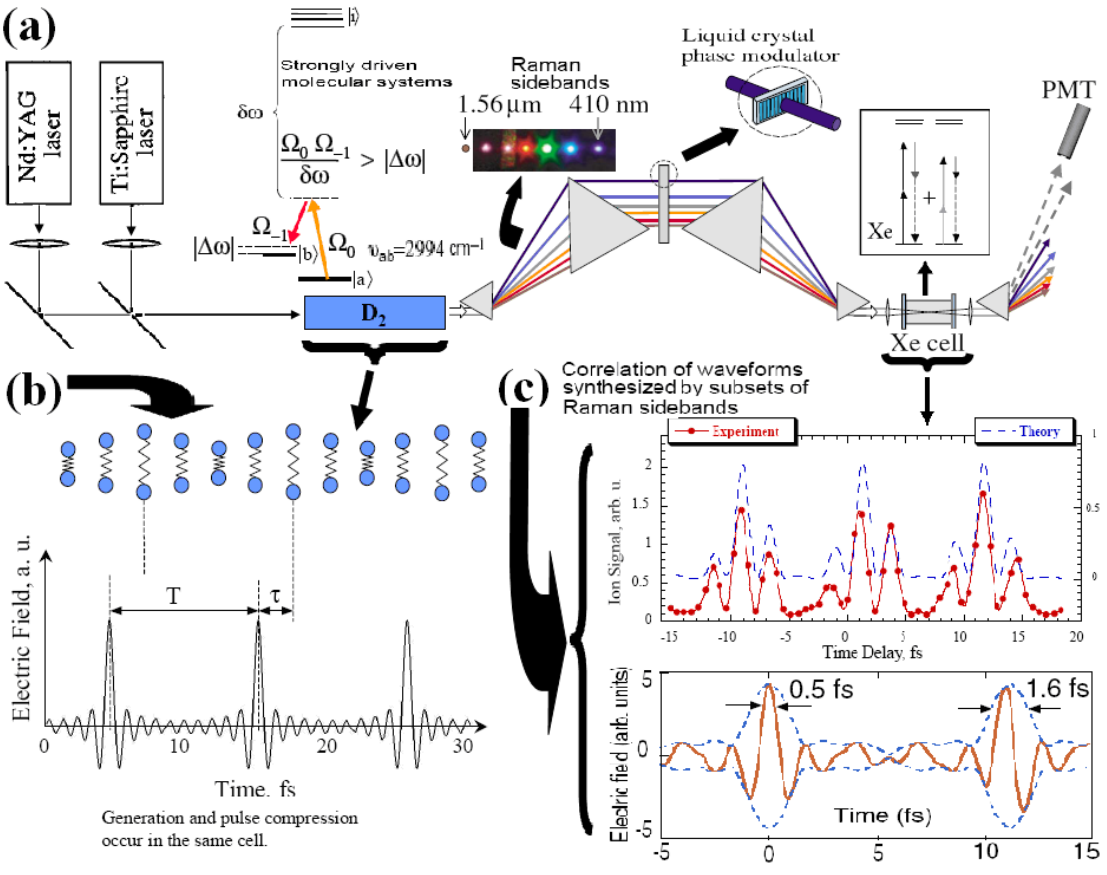

Fig. 1.3. a) Experimental setup for temporal synthesis and characterization of single-cycle pulses. b) Modulation and synchronization of the pulse train with respect to the molecular oscillation. c)

Photoionization of xenon for characterization of synthesized single-cycle pulse train [2,3,4,13,14,24,28,31,32,35,36].

Classically, this interaction can be pictured [Fig. 1.3(b)] as driving a harmonic oscillator near its resonance at the beat note frequency of the two lasers [2]. In this manner a very efficient molecular motion mixes with the two applied fields is prepared to produce new coherent frequencies [2]. Molecular motion, either in phase with the driving force (Raman detuning below resonance) or antiphased (Raman detuning above resonance) [Fig. 1.3(a)], in turn modulates the driving laser frequencies [32]. In its simplest terms, molecular modulation is very much similar to electro-optic modulation. The only difference is that molecular modulation occurs at the frequencies at 5 orders of magnitude larger [36]. What the coherent molecular motion does is to modulate the refractive index of the medium. If we consider the molecules of deuterium (D_2) [Fig. 1.3(b)], when they are stretched, they are easier polarizable [36]. Thus the refractive index of a medium composed of stretched molecules is larger than the refractive index of a medium composed of compressed molecules [36]. If the molecules in a sample oscillate in unison, the macroscopic index of refraction of that medium is modulated sinusoidal with the frequency of the molecular motion [35]. So, the molecular modulation is essentially due to the production of Stokes and anti-Stokes Raman sidebands of a special regime of Raman scattering with maximal coherence [35].

The Raman generator in Fig. 1.3(a) is constructed by driving the fundamental vibrational transition of D_2 by two transform-limited laser pulses, one from Nd: Yag laser at 1.064 μm and the other from a Ti:Sapphire laser at 807 nm, such that their

frequency difference is approximately equal to the transition frequency of 2994 cm^{-1} [24]. The energy and pulse width of the 1.064 μm beam are 70 mJ and 10 ns. For the 807 nm beam, these quantities are 60 mJ and 15 ns [24]. Both have a repetition rate of 10 Hz and are combined and loosely focused into a 50 cm long D_2 cell [24]. The output after the deuterium cell is white light and the generated spectrum, which can be observed by dispersing the beam with a prism [2], consists of up to seventeen sidebands and extends over many octaves of optical bandwidth (from 2.95 μm in the infrared to 195 nm in the ultraviolet) [3]. As it is seen in Fig. 1.3(a), only the seven of these generated sidebands are used and the other frequencies are blocked [2]. The good mutual coherence across the spatial and temporal profiles of generated Raman sidebands by molecular modulation, allows them to be recombined spatially after the phase adjustment with a liquid crystal phase modulator and spectral modification techniques to be used to synthesize specified femtosecond time structures in a Xe target cell [see Fig. 1.3(a)] [24]. The desired pulse is synthesized in this focal region of overlapping sidebands inside the chamber where four-wave mixing serves as a pulse shape diagnostic [see Fig. 1.3(c)] [2]. Focusing the sidebands into the chamber produces a very weak UV signal in the range of picojoules at several discrete frequencies resulting from the four-wave mixing nonlinear process in Xe [2]. The magnitude of the ion signal depends on the intensity of the synthesized pulse [2]. The shortest possible pulse that can be synthesized also has the highest possible intensity [2]. So, the UV signal serves as feedback to the spatial light modulator for providing an adaptive phase adjustment of the seven Raman sidebands [2]. Fig. 1.3(c) shows the

cross-correlation trace of the synthesized pulse and the predicted single-cycle electric field profile from this correlation [2,24].

The second and the very recent experimental approach on the generation of single-cycle of light pulses makes use of the erbium-doped fiber laser technology [14].

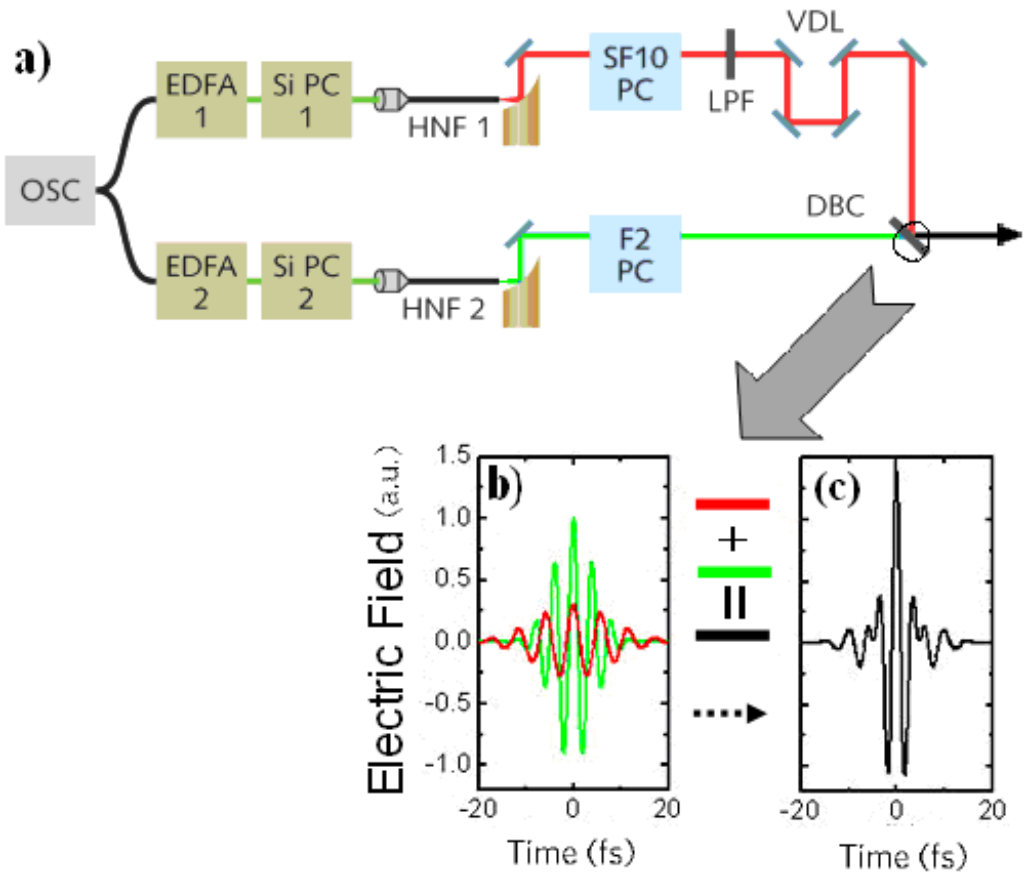

Fig. 1.4. a) Set-up of a single-cycle fiber laser system. OSC: femtosecond erbium-doped fiber oscillator, EDFA: erbium-doped fiber amplifier, Si PC: silicon prism compressor, HNF: bulk highly nonlinear fiber for tailored supercontinuum generation, F2 / SF10 PC: pulse compressors with F2 and SF10 Brewster prisms, LPF: low-pass filter (cutoff wavelength 1600 nm), VDL: variable delay line, DBC: dichroic beam combiner. The divergent output leaving each HNF end facet is collimated with off-axis parabolic mirrors [4]. b) Temporal oscillations of the electric field of two synchronized ultrashort light pulses with different center frequencies [37]. c) The coherent superposition of the transients. They are combined in space and time such that the central field maxima are exactly in sync with each other. In

this way, these regions get amplified. Due to the different frequencies, destructive interference sets in already during the oscillation cycles before and after the central maximum [4,14,37,38].

An innovative way for the construction of single-cycle of light through the coherent superposition of two non-overlapping spectra of separate pulse trains using this technology is reported in [4] [see Fig. 14(a)]. Since the possibility to achieve broader bandwidth and shorter pulse duration is to coherently superimpose [see Figs. 1.4(a), 1.4(b)] separated spectra from independent broadband lasers at different center wavelengths [39], the coherent interference between the outputs of two mode-locked lasers has already been tried to be used in several studies, but timing jitter has always prevented the success [38]. To combat this drawback, as it is seen in Fig. 1.4, it is the first time that a beam from a mode-locked femtosecond erbium-doped fiber oscillator operating at a repetition rate of 40 MHz is split into two branches and used as seed pulses for two different parallel femtosecond erbium-doped fiber amplifiers [4]. In each branch the average power of the femtosecond pulse train is amplified to 330 mW. Using the same oscillator as a seed for deriving both spectra provides an achievement in the need to reduce the residual timing jitter between the two pulse trains to a level of 43 as [14]. In each branch, the pulses are compressed to pulse durations of 120 fs in a silicon prism sequence [39]. Subsequent supercontinuum generation in highly nonlinear fiber assemblies lead to tailor cut spectra with center wavelengths of 1125 nm (dispersive wave) and 1770 nm (soliton), respectively [39]. The two components are then combined with a dichroic mirror. The temporal overlap is aligned with a piezo-controlled delay stage in one branch [39]. At the optimum relative temporal position between the two components of $\Delta t=0$ fs, constructive interference arises

exactly for the central field maxima of each pulse, whereas the rest of both transients superimposes destructively which indicates the formation of a single cycle pulse [4].

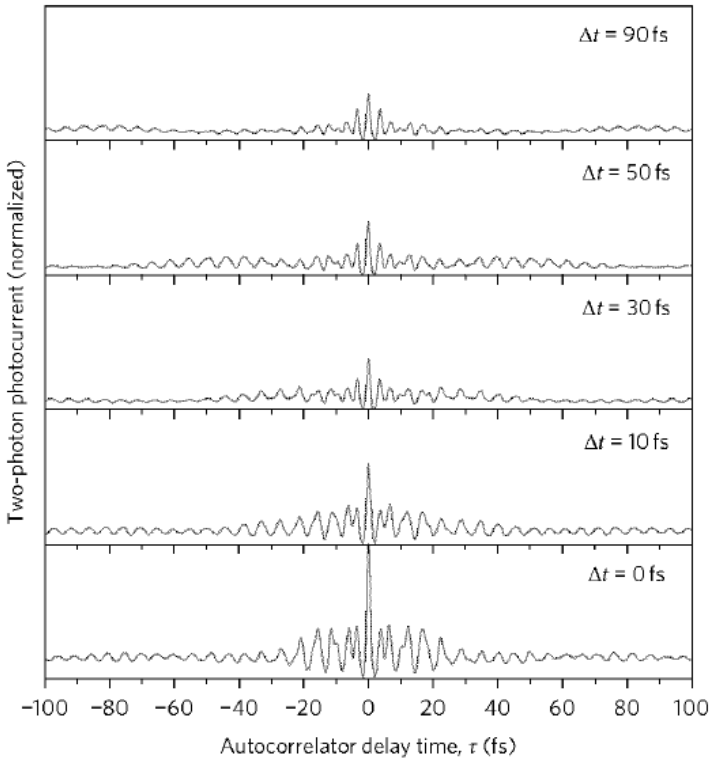

Fig. 1.5. Fringe-resolved second-order autocorrelations for two-photon signal from a GaAs photodiode versus different time delay Δt between dispersive wave and soliton. At the optimum overlap (Δt=0) the signal features an isolated central maximum, indicating the formation of a single-cycle pulse with duration 4.3 fs [4].

Due to the advent of these new experimental studies, the need for understanding the interaction of a USCP with the medium through which it is propagating in is an important and timely topic [40,41,42,43,44,45,46]. The interaction of a laser pulse with matter involves the interaction of the incident electric field with the electrons of the material. Basic physics of the pulse-matter interaction depends strongly on the ratio of the pulse duration and the characteristic response time of the medium (as well

as on the pulse intensity and energy). This ratio is the key term in the polarization response of the medium from a classical point of view. The goal of this thesis is to provide the mathematical model for the interaction dynamics of a USCP with a bound electron without ionization for the first time. This study is concerned with the linear polarization response of dispersive materials under USCP excitation where the electric field strength is low enough to not produce ionization. Since the energy is below the ionization threshold of the medium, there is not any plasma effect during the interaction of the applied field with the matter. Understanding the linear polarization response is crucial in order to formulate a realistic field integral. This realistic field integral will provide a more realistic propagation model of optical pulses through dispersive media [47-67].

CHAPTER 2

MODIFIER FUNCTION APPROACH FOR USCP INTERACTION IN TIME DOMAIN WITH A BOUND ELECTRON WITHOUT IONIZATION

2.1 Mathematical Model

In order to make an original contribution for the analysis of the interaction of an ultrashort single-cycle pulse (USCP) with a bound electron without ionization, first it is necessary to find a realistic model for a USCP. Such pulses have a rather different structure from conventional modulated quasi-monochromatic signals with a rectangular or Gaussian envelope [40,41,42,43]. Due to the following main reasons associated with USCPs, combination of Laguerre functions and Hermitian polynomials (Mexican Hat) are used in this study for modeling applied EM field:

i) Arbitrary transient steepness: The rising and the falling times of the signal can be unequal.

ii) Varying zero spacing: The distances between zero-crossing points may be unequal.

iii) Both the waveform envelope and its first spatial, second spatial and temporal derivatives are continuous.

iv) Arbitrary envelope asymmetry: USCP waveforms can be classified conventionally for two groups.

1) The sharply defined zero-crossing point at the pulse leading edge as initial point (combination of Laguerre functions).

2) The sharply defined narrow maximum against a background of comparatively long tails (Hermitian polynomials – Mexican Hat). [40,41,42,43].

Although delta function or the Heaviside step function are widely used, they assume zero signal duration and zero relaxation time. These assumptions are not suitable for modeling the waveform of a USCP. There are some other more realistic models, such as modulated Gaussian or rectangular transients, but these models assume equally spaced zeros which is not suitable for a USCP, neither [40,41,42,43].

The combination of Laguerre functions for defining the spatiotemporal profile of a USCP is defined as $E_m(t) = B(L_m(t) - L_{m+2}(t))$ where $L_m(x) = (\exp(x/2)/m!)\frac{d^m}{dx^m}[\exp(-x)x^m]$ is a single Laguerre function with order m and $x = (t - zc^{-1})/t_0$. Here, B is normalization constant, c is the velocity of light in vacuum, z is the propagation direction and t_0 is the time scale of the pulse. In this study, the combination of 2nd and 4th order Laguerre functions are used to define a single USCP:

$$E_2(\alpha) = \exp\left(-(7.5\alpha)^2\right)\left[-\frac{1}{24}\alpha^4 + \frac{15}{24}\alpha^3 - \frac{5}{2}\alpha^2 + 2\alpha\right], \qquad (2.1)$$

where the phase term is defined as $\alpha = (t - \phi - zc^{-1})/t_0$. Here, ϕ is the initial phase, z is the spatial coordinate in the propagation direction of the pulse and t_o is the time

scale of the pulse. For Laguerre USCP, $\phi = 4x10^{-16}$, $z = 5x10^{-9}m$ and $t_o = 10^{-15}$ seconds. Here, ϕ and z are chosen arbitrarily. With these values, we have the phase term $\alpha = {}^{t}\!/_{t_o} - 0.4167$. So, we obtain the Laguerre USCP [Fig. 2.1(a)] in time domain as:

$$E(t) = \exp\left(-\left(7.5\left(\frac{t}{t_o} - 0.4167\right)\right)^2\right)\left[-\frac{1}{24}\left(\frac{t}{t_o} - 0.4167\right)^4 + \frac{15}{24}\left(\frac{t}{t_o} - 0.4167\right)^3 - \frac{5}{2}\left(\frac{t}{t_o} - 0.4167\right)^2 + 2\left(\frac{t}{t_o} - 0.4167\right)\right]. \tag{2.2}$$

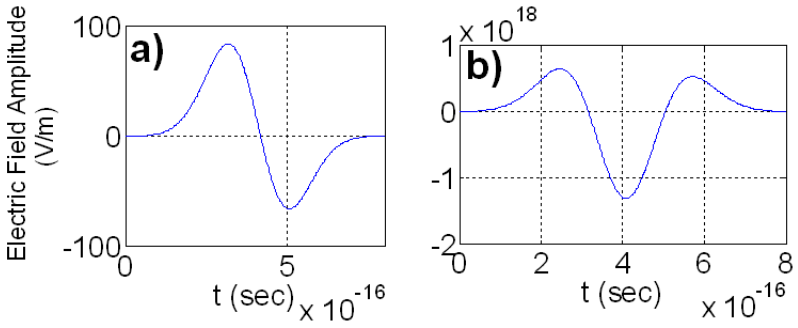

Fig. 2.1. (a) Applied Laguerre USCP with pulse duration τ_p=8x10^{-16} seconds. (b) 1st derivative (V/m.sec) of the Laguerre USCP.

Fig. 2.1(b) shows the first derivative of the applied field and it is seen that the analytical expression $E(\alpha)$ in Eq. 2.1 satisfies the conditions of arbitrary transient steepness and arbitrary envelope asymmetry. From Fig. 2.1(a), it is also seen that it satisfies the condition of varying zero spacing for a USCP. In addition to these, time profile of the Laguerre USCP almost satisfies the integral property:

$$\int_0^\infty E(\alpha)d\alpha = 0. \tag{2.3}$$

For the Hermitian (Mexican Hat) USCP [Fig. 2.2(a)], the following definition is used:

$$E(\alpha) = (1-\alpha^2)\exp(-\alpha^2/2), \tag{2.4}$$

where, $\phi = 4x10^{-15}$, $z = 5x10^{-9}m$ and $t_o = 10^{-15}$ seconds. With these values, we have the phase term $\alpha = t/t_o - 4.0167$. So, we define the Hermitian USCP [Fig. 2.2(a)] in time domain as:

$$E(t) = \left(1-\left(\frac{t}{t_o}-4.0167\right)^2\right)\exp\left(-\left(\frac{t}{t_o}-4.0167\right)^2/2\right) \tag{2.5}$$

Fig. 2.2(b) illustrates that the Hermitian pulse satisfies the above concerns.

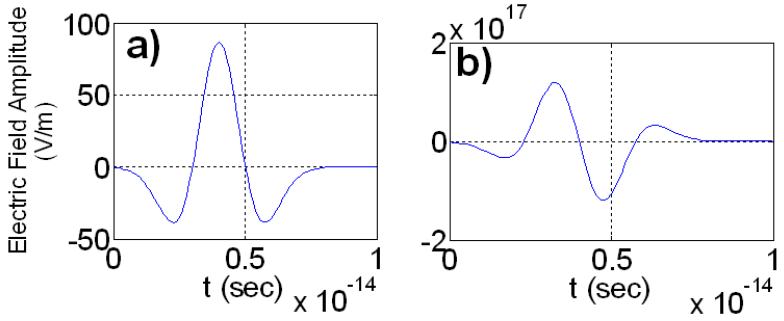

Fig. 2.2. (a) Applied Hermitian USCP with pulse duration τ_p= 8x 10^{-15} seconds. (b) 1st derivative (V/m.sec) of the Hermitian USCP.

In addition to the question how to formulate ultrashort single cycle transients, it is also natural to ask how these pulses propagate in optical medium. In this study, USCP

means the smallest possible single cycle piece (unity source) of a wave packet. It is the part of an actual carrier field and does not contain any other carrier fields in itself. For a USCP, it is difficult to introduce the concept of an envelope and it is not possible to define a group velocity. For such short pulses the distinction between carrier oscillations and slowly varying envelope (SVE), which have two different temporal scales that are peculiar to quasi-monochromatic pulses, becomes diffuse or meaningless [47,68,69,70]. Jumping from many cycle optical waves to single cycle optical pulses in dealing with light-matter interaction, the mathematical treatments should be revised. The traditional analysis of pulsed EM phenomena is questionable [40,41,42,43]. If the applied field is a USCP, the shortest possible field as explained above, then it is impossible to separate the applied source into pieces to find the effect of each part (or piece) by superposing as being suggested in the models explained in many fundamental textbooks [71].

In order to understand the USCP-medium interaction phenomenon, we must acquire certain special features such as operating directly with Maxwell equations beyond the scope of Fourier representations [40,41,42,43]. Since the situations occur where the time scale of the pulse is equal or shorter than the relaxation time of the medium, material has no time to establish its response parameters during the essential part of the pulse continuance [58,66,72,73,74]. These parameters, which govern the polarization response of the media, change their values during the pulse continuance [58,72]. Thus, solutions of Maxwell equations with time-dependent coefficients are required for the analysis of the wave dynamics [66,74].

In our study, we consider an approach such that under a single USCP excitation, the change in the relative position of a bound electron to its parent atom without ionization will change the amplitude of the dipole in the atom and so forth the instantaneous polarization. As a result of this fluctuation in the polarization, the index of refraction will change in the duration of the single USCP excitation during which the propagation dynamics of the same applied USCP and the other USCPs coming after the first one will be evaluated. So physically, we consider a case where the medium is including the source. This is a common situation especially in optical communication. In addition to this, we can associate this approach to some diagnostic techniques in ultrafast optics such as pump-probe experiments where both pump and probe pulses propagate and evaluate the time varying physical parameters of the medium. But before diving into Maxwell equations, we have to figure out how the polarization response of the medium must be handled for the interaction of a USCP EM field with a bound electron. Understanding the polarization response of the material under the excitation of a USCP EM field is one of the most important, not clearly answered yet, core question of today and near future ultrafast laser engineering.

Polarization is a crucial physical phenomenon, especially for optical communication, since it defines the change in the index of refraction in the material due to the applied field [58,72,73,75,76]. In terms of permittivity, we can write index of refraction (for a nonmagnetic material) as:

$$n = \left(1 + {P_{pol}(t)}/{\varepsilon_o E(t)}\right)^{1/2}, \tag{2.6}$$

[see Ref. [77], pp: 68-70 and Ref. [78], pp: 69-70 for the justification of Eq. (2.6)] where ε_o is the permittivity of free space, $E(t)$ is the applied electric field, and $P_{pol}(t)$ is the electronic polarization. The polarization response of the medium gives the change in the index of refraction. This change or this polarization response affects the temporal and spatial evaluation (Fig. 2.3) of the propagating pulse [1,23,79].

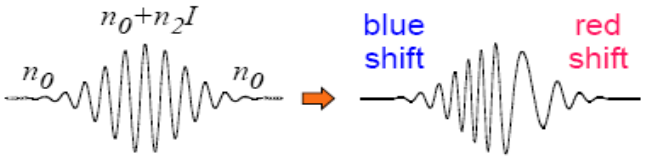

Fig. 2.3. Schematic representation of self-modulation (pulse chirping). Although we are interested in the low intensity applied fields for linear polarization in this study, temporal dependence of the intensity profile of the applied field can still cause a temporal dependence in the refractive index [79].

The starting point of all these dynamics is the inhomogeneous wave equation:

$$\frac{\partial^2 E(z,t)}{\partial z^2} - \frac{1}{c_0^2}\frac{\partial^2 E(z,t)}{\partial t^2} = \mu_o \frac{\partial^2 P_{pol}}{\partial t^2}, \tag{2.7}$$

where the polarization is the source term of the governing differential equation. In order to find the polarization, we must find the oscillation field (displacement) of the bound electrons. According to the Lorentz damped forced oscillator model:

$$m_e \frac{d^2 x(t)}{dt^2} + m_e \gamma_o \frac{dx(t)}{dt} + k_o x(t) = q_e E(t), \tag{2.8}$$

$x(t)$ is the time dependent displacement or the oscillation field of a bound electron with respect to the applied field $E(t)$, γ_o is the damping constant, k_o is the spring constant of the material and m_e is the mass of electron.

For USCP excitation, unlike the long pulse excitation fields, the response (oscillation) of the electron must be handled in a different manner. Since, both due to the mass of inertia of the electron and the shortness of the USCP compared to the relaxation time of the medium, the electron will not sense the applied field exactly at the leading edge point of the pulse. The response of the electron to the applied field will increase gradually. During this sense, the electron will not follow the oscillation profile of the applied electric field. So, the oscillation field of the electron will not only have a difference in the phase but also will have a different time profile (time-dependency) with the applied field. In regular cases, if the applied field is in the form of e^{jwt} time-dependency, then we assume that the oscillation of the electron will be in the same time-dependency form. In the literature, Lorentz oscillator model is directly used in e^{jwt} time-dependency [80]. But for a USCP excitation, not only the time-dependency e^{jwt} is not valid, but also the oscillation field will have a different

waveform than the applied field waveform (time-dependency). This means that, the $x(t)$ term in Eq. (2.8), that is the oscillation field of the electron, will have a modified form of time-dependency with respect to the applied USCP. In order to define the modified function $x(t)$, we developed a new time domain technique that we call "Modifier Function Approach". In this approach, we define the oscillation field of the electron as the multiplication of the applied USCP with the modifier function:

$$x(t) = x_o(t)E(t), \tag{2.9}$$

where $x_o(t)$ is the modifier function. It has a unit of (meter)^2/volt which is equivalent to coulomb*meter/newton. So physically, modifier function defines dipole moment per unit force. Plugging Eq. (2.9) into Eq. (2.8), we obtain

$$m_e \frac{d^2(x_o(t)E(t))}{dt^2} + m_e\gamma_o \frac{d(x_o(t)E(t))}{dt} + k_o(x_o(t)E(t)) = q_e E(t). \tag{2.10}$$

After a few manipulations, we may unite this as Eq. (2.13):

$$\begin{aligned} &m_e \frac{d^2x_o(t)}{dt^2}E(t) + 2m_e \frac{dx_o(t)}{dt}\frac{dE(t)}{dt} + m_e x_o \frac{d^2E(t)}{dt^2} + m_e\gamma_o \frac{dx_o(t)}{dt}E(t) + \\ &m_e\gamma_o x_o(t)\frac{dE(t)}{dt} + k_o x_o(t)E(t) = q_e E(t), \end{aligned} \tag{2.11}$$

$$m_e E(t)\frac{d^2x_o(t)}{dt^2} + m_e\left(2\frac{dE(t)}{dt} + \gamma_o E(t)\right)\frac{dx_o(t)}{dt} + m_e\left(\frac{d^2E(t)}{dt^2} + \gamma_o\frac{dE(t)}{dt} + \frac{k_o}{m_e}E(t)\right)x_o(t) = q_e E(t) \tag{2.12}$$

$$\frac{d^2x_o(t)}{dt^2}+\left(\frac{2}{E(t)}\frac{dE(t)}{dt}+\gamma_o\right)\frac{dx_o(t)}{dt}+\left(\frac{1}{E(t)}\frac{d^2E(t)}{dt^2}+\frac{\gamma_o}{E(t)}\frac{dE(t)}{dt}+\frac{k_o}{m_e}\right)x_o(t)=\frac{q_e}{m_e}. \quad (2.13)$$

We can briefly write Eq. (2.13) as:

$$\frac{d^2x_o(t)}{dt^2}+P(t)\frac{dx_o(t)}{dt}+Q(t)x_o(t)=\frac{q_e}{m_e}, \quad (2.14)$$

where

$$P(t)=\frac{2}{E(t)}\frac{dE(t)}{dt}+\gamma_o, \quad (2.15)$$

$$Q(t)=\frac{1}{E(t)}\frac{d^2E(t)}{dt^2}+\frac{\gamma_o}{E(t)}\frac{dE(t)}{dt}+\frac{k_o}{m_e}. \quad (2.16)$$

It is seen at Eq. (2.14) that it has a similar form with a Hill type equation where for a regular Hill equation, $P(t)$ and $Q(t)$ terms are periodic and the right side is zero. A linear equation of this type occurs often when a system exhibiting periodic motion is perturbed in some way [81]. This type of equation was first derived by G.W. Hill to describe the effect of perturbations on the orbit of the Moon, and it occurs in many other places in physics, including the quantum motion of electrons in a periodic potential of a crystal [81]. The band theory of solids is based on a similar equation, as is the theory of propagating electromagnetic waves in a periodic structure [81]. Other applications include parametric amplifiers. Although $P(t)$ and $Q(t)$ terms are periodic in a Hill equation, in our case they are not. So, in our model, Eq. (2.14) is a Hill-like

equation which has a dc source on its right side and a time-dependent damping coefficient (2.15) and a time-dependent spring coefficient (2.16) in terms of a damped forced oscillator model. The objective of Eq. (2.14) is to find the modifier function which can be then used to define the oscillation field (polarization response) of the material. Due to the time-dependent damping and spring coefficients, the modifier function is totally coupled with the time dependency or time profile of the applied field.

Eq. (2.8) could also have been solved directly in the temporal domain, in which case we would have lost the analogy with the Hill-like equation. But the appropriateness of using the more complicated approach with the modifier function has solid physical reasons. In the case of a USCP excitation, the polarization response of the material is not unique all through the pulse continuance. Due to the shortness of the duration of the applied USCP comparing to the relaxation time of the bound electron, the interaction dynamics and the ability of the material to sense and follow the applied USCP field during its continuance will be completely different than the conventional matter-field interaction approach. In Eq. (2.8), physical parameters (damping and spring coefficients) are constant. However, the interaction dynamics will not be constant during the USCP excitation. So, in order to penetrate the effect of the applied field into the oscillator model via these physical parameters to have a better understanding of the oscillation response of the material under USCP excitation, we must find the definition of these physical parameters in terms of the applied field and the physical constants of the system (material). Eq. (2.15) and Eq. (2.16) are these definitions. They are being used in Eq. (2.14) to find the modifier function which has

been embedded into Eq. (2.8). The physical dimension of the modifier function is a dipole moment per unit force. It frames the time dependency and the phase delay of the oscillation field of the bound electron under USCP excitation.

2.2 Numerical Results and Discussions

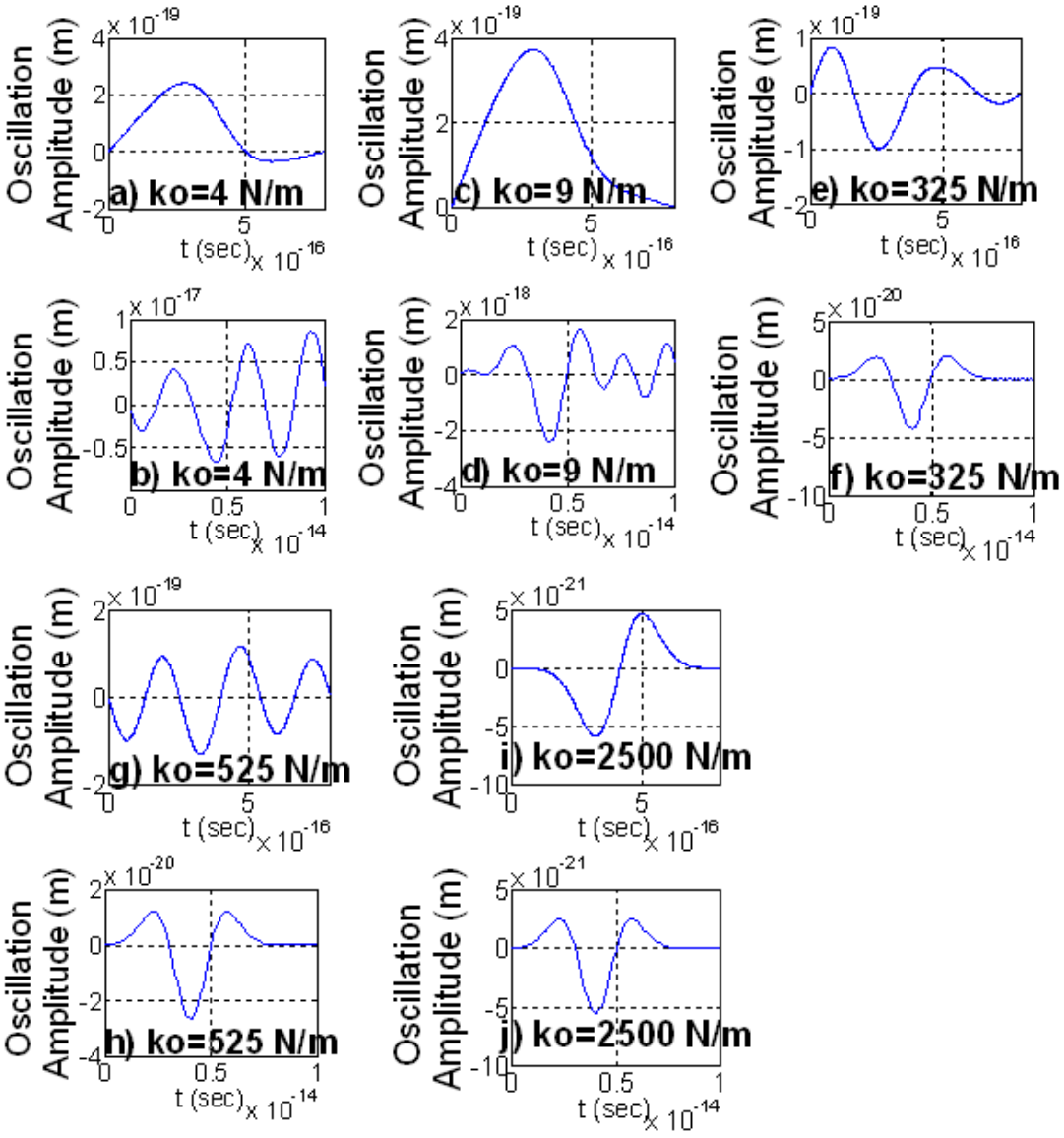

Fig. 2.4. Bounded electron motion under Laguerre USCP excitation ((a), (c), (e), (g), (i)) and Hermitian USCP excitation ((b), (d), (f), (h), (j)) for various values of spring constant (k_o) with a fixed damping constant ($\gamma_o = 1x10^{14}$ Hz).

In Fig. 2.4, different interaction characteristics of Laguerre and Hermitian pulses are shown for a fixed, relatively low value of damping constant ($\gamma_o = 1x10^{14}$ Hz). Due to the definition: $w_0 = \sqrt{k_o / m_e}$, (m_e is the mass of electron, k_o is the spring constant for bound electron), the free oscillation frequency of material is in UV range for spring constant values of 4 N/m, 9 N/m, 325 N/m, 525 N/m [Figs. 2.4(a), 2.4(b), 2.4(c), 2.4(d), 2.4(e), 2.4(f), 2.4(g), 2.4(h), 2.13(a)], 650 N/m [Fig. 2.13(b)] and 750 N/m [Figs. 2.5(b), 2.13(c)]. For spring constant values of 1500 N/m [Fig. 2.5(c)], 2500 N/m [Figs. 2.4(i), 2.4(j)] and 7500 N/m [Fig. 2.13(d)], the free oscillation frequency is in X-ray range. As it is seen in Fig. 2.4, the Hermitian interaction has a more tendency to oscillation than the Laguerre interaction for relatively low values of spring constant [see Figs. 2.4(a), 2.4(b), 2.4(c), 2.4(d)]. As the spring constant is increased, Laguerre interaction gains a more oscillatory profile [see Figs. 2.4(e), 2.4(g)] while the oscillation due to the Hermitian pulse interaction stabilizes and its time profile settles down into the inverted phase time profile of the excitation pulse (inverted Mexican Hat) [see Figs. 2.4(f), 2.4(h), 2.4(j)]. Here, the amplitude of oscillation or the amplitude of trembling-like motion of the electron is in the range of 10^{-20} m – 10^{-21} m which is in the scale of electron radius length. Finally, as the spring constant is increased to relatively higher values, the Laguerre interaction settles down into the inverted phase time profile of the excitation pulse, too (inverted Laguerre pulse) [see Fig. 2.4(i)]. Fig. 2.4 shows a very clear distinction between the interaction characteristics of Laguerre and Hermitian USCPs until the spring constant is 2500 N/m (after this value, we obtain only the inverted phase time profile of the excitation source for the oscillation). The oscillation characteristics of bound electron under different single USCP sources originates from

modifier function approach. The Hill-like equation, which is the result of the modification on the classic Lorentz damped oscillator model with the modifier function approach, causes the time varying physical parameters to come into play during the interaction process. Since these physical parameters (time varying damping and spring coefficients) are absolutely source dependent, they behave differently in the pulse duration of each different USCP source. As a result of this, we see different oscillation profiles for a bound electron under a single Laguerre and Hermitian USCP excitations.

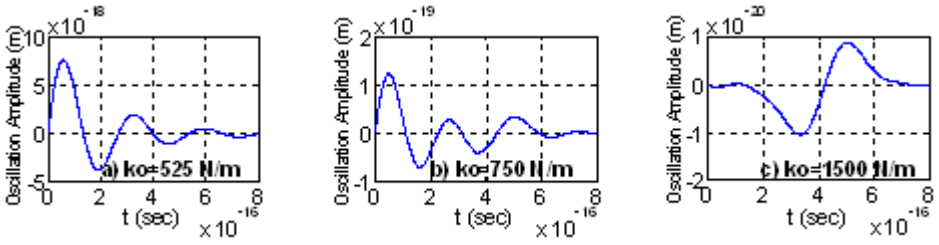

Fig. 2.5. Laguerre pulse excitation oscillations for damping constant: $\gamma_o = 1x10^{16}$ Hz.

In Fig. 2.5, response of a bound electron is shown for a Laguerre pulse excitation for varying values of spring constant with a fixed, relatively higher damping constant value ($1x10^{16}$) than the previous case (Fig. 2.4). An interesting feature here in Fig. 2.5(a) and Fig. 2.4(g) is that although they are at the same spring constant value, they show different oscillation characteristics. Due to a higher dampimg coefficient in Fig. 2.5(a), while the oscillation attenuates quicker at the second half cycle of the Laguerre USCP than in Fig. 2.4(g), it hits to a higher peak at the first half cycle of the excitation pulse than in Fig. 2.4(g). So, for a reasonable value of spring constant, while relatively higher damping coefficient makes the first half cycle of the Laguerre USCP more

efficient in the means of interaction, it makes the second half cycle less efficient. In order to compare oscillation results more detailly between Figs. 2.5(a) and 2.4(g), it is

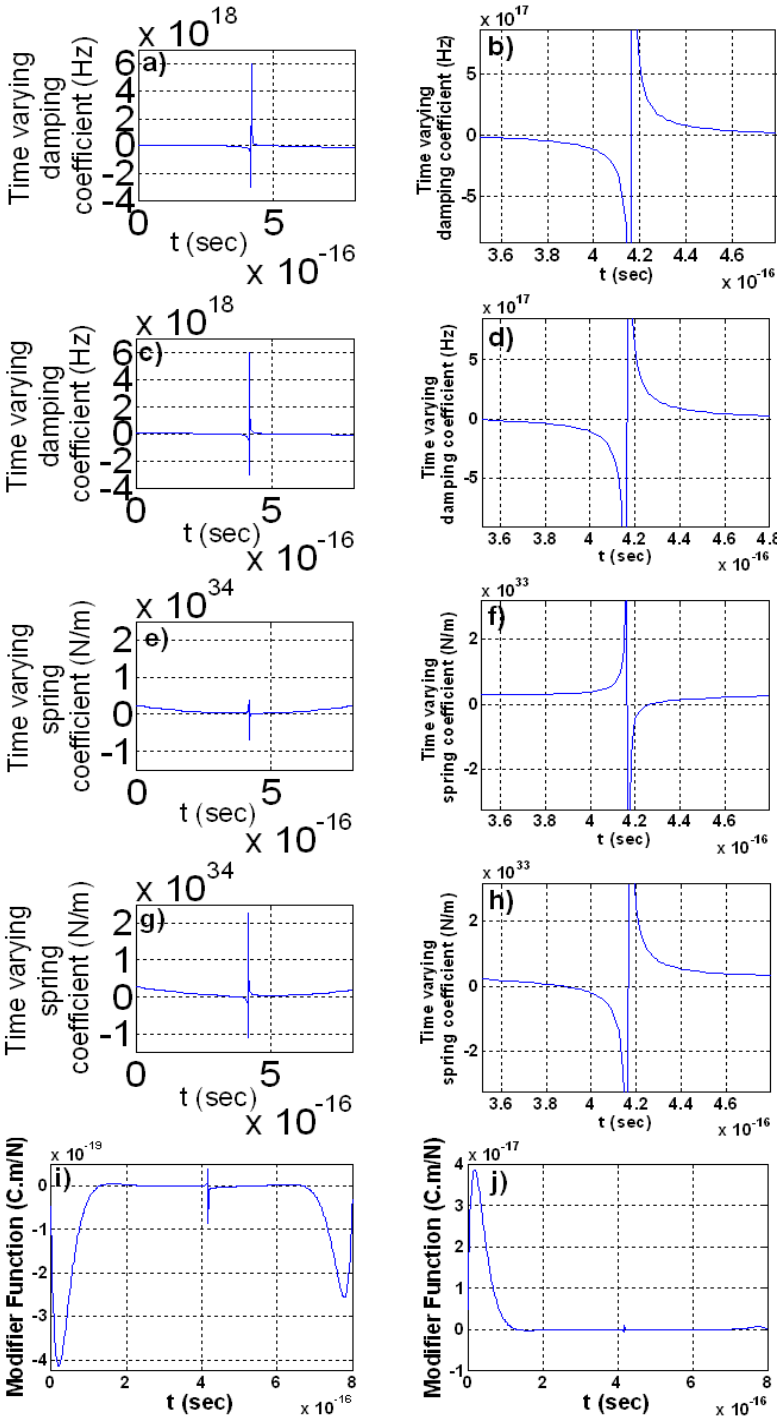

Fig. 2.6. Laguerre Pulse Excitation physical parameter solutions for spring constant $k_o = 525$ N/m. (a), (b), (e), (f) and (i) are the solutions of Fig. 2.4(g) (damping constant $\gamma_o = 1x10^{14}$ Hz). (b) and (f) are the magnified views of (a) and (e) respectively. (c), (d), (g), (h) and (j) are the solutions of Fig. 2.5(a) (damping constant $\gamma_o = 1x10^{16}$ Hz). (d) and (h) are the magnified views of (c) and (g) respectively.

necessary to look at their physical parameter solutions such as time varying damping and time varying spring coefficients. As it is explained above, these time varying

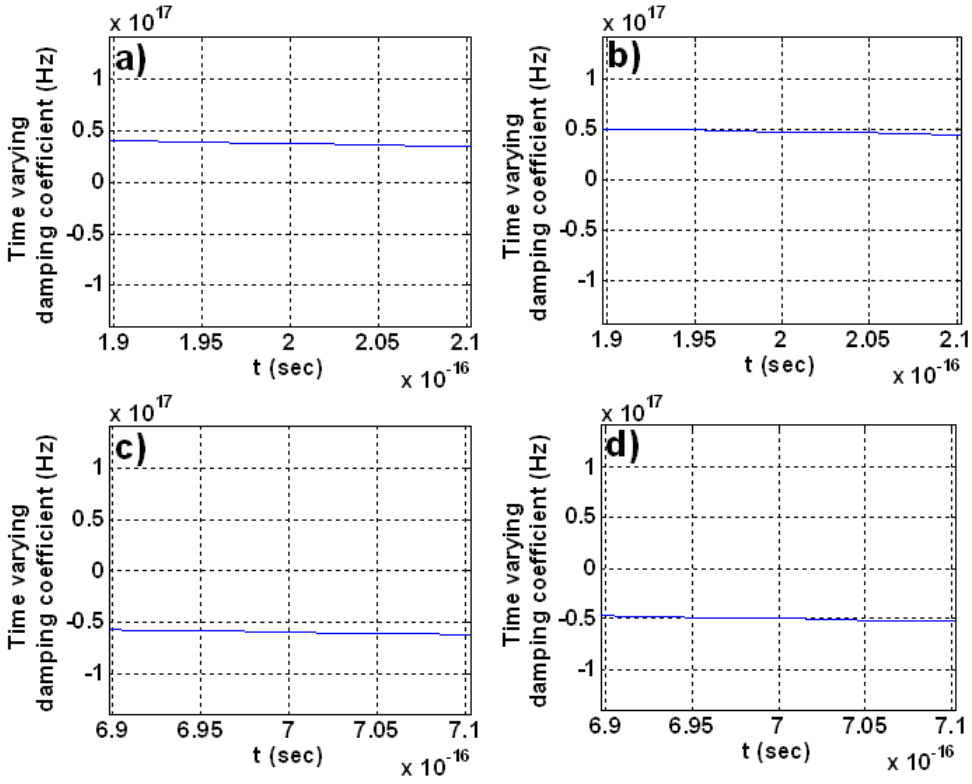

Fig. 2.7. (a) – (b): Magnified views of left wings of Figs. 2.6(a) - 2.6(c). (c) – (d): Magnified views of right wings of Figs. 2.6(a) - 2.6(c).

parameters come into play due to the nature of "Modifier Function Approach". In Fig. 2.6, time varying damping coefficient, time varying spring coefficient and the

modifier function solutions of Figs. 2.4(g) and 2.5(a) are shown respectively for two different damping constant values with a fixed spring constant at 525 N/m. In Figs. 2.6(a) and 2.6(c), a sudden jump is seen in the time varying damping coefficient profiles at the time point where the excitation pulse changes its polarization direction. Although they look identical, the magnified views [see Figs. 2.7(a), 2.7(b), 2.7(c), 2.7(d)] of the left and right wings of the damping coefficient show the difference between two different damping constant cases. Here, the left wing corresponds to the first half cycle, right wing corresponds to the second half cycle of the Laguerre excitation pulse. Comparing the amount of the change on the y-axis with the time duration on the x-axis between Figs. 2.7(a) – 2.7(b), and 2.7(c) – 2.7(d), it is easy to see the reasonable amount of difference to affect the solution of modifier function [see Figs. 2.6(i), 2.6(j)]. For time varying spring coefficients [see Figs. 2.6(e), 2.6(g)], a significant difference is seen in the time profile although the spring constant values are the same for both cases. The jump in Fig. 2.6(g) hits a higher peak than the jump in Fig. 2.6(e). This can be a reasonable explanation for a relatively low oscillation tendency in the second half cycle of Fig. 2.5(a) than the Fig. 2.4(g). It can be said that, due to the dissipation of higher energy, this jump causes a lower oscillation profile for the bound electron during its interaction with the second half cycle of the Laguerre pulse in Fig. 2.5(a) than in Fig. 2.4(g). In Fig. 2.5(c), as the spring constant is increased to relatively higher values, same as in Fig. 2.4(i), the oscillation profile settles down into the inverted time phase profile of the excitation pulse. Different from Fig. 2.4(i), the oscillation settles down at a relativley lower spring constant value. So,

it can be said that, for a higher damping constant, a lower spring constant is enough to stabilize the oscillation profile in time domain.

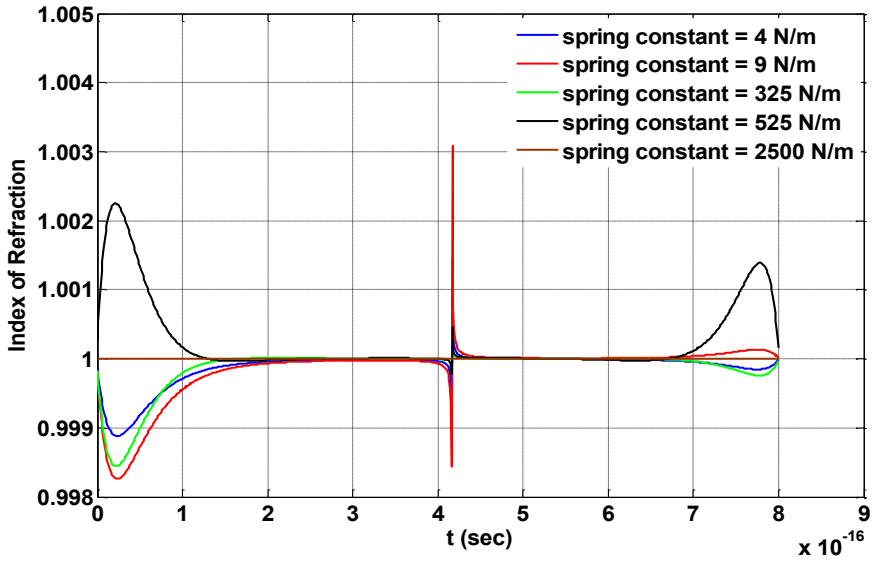

Fig. 2.8. Time dependent index of refraction during the interaction of a single Laguerre USCP with a bound electron without ionization for different spring constant values with a fixed damping constant value ($\gamma_o = 1x10^{14}$ Hz). It is obtained from Eq. (2.6) where $P_{pol}(t) = Nq_e x(t)$. Here $N = 6.02x10^{23}$ and q_e is the electron charge.

Fig. 2.8 shows the perturbation effect of an applied single Laguerre USCP on the index of refraction during its continuance for varying spring constants with a fixed damping constant value. As it is clearly seen in Fig. 2.8, for all spring constant values except the relatively higher case (2500 N/m), there are three regions where the perturbation effects are dominant. These are the trailing and leading regions of the pulse and the time point where the applied electric field changes its polarization sign. The change in the index of refraction around the trailing and leading edges is not as sharp as the change at the point where the polarization sign of the field changes. To

see this sudden effect more clearly, the zoomed view of this region is shown in Fig. 2.9.

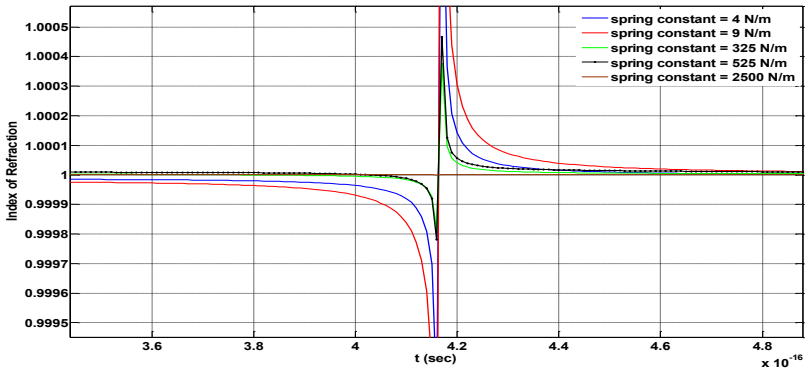

Fig. 2.9. The jump in the time dependent index of refraction where the electric field changes its polarization sign.

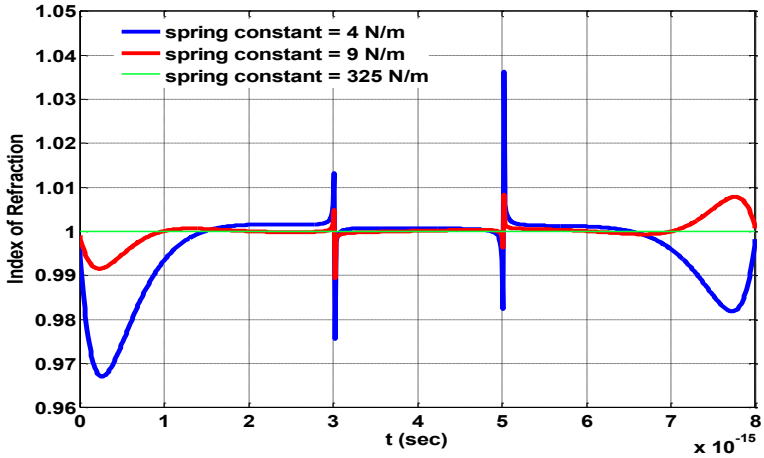

Fig. 2.10. Time dependent index of refraction during the interaction of a single Hermitian USCP with a bound electron without ionization for different spring constant values with a fixed damping constant value ($\gamma_o = 1x10^{14}$ Hz).

The same type of perturbation behavior seen in Fig. 2.8, is seen in the interaction of a single Hermitian USCP with a bound electron, too (see Fig. 2.10). Both of these

figures have the same damping constant value. The only difference in the time dependent perturbation of index of refraction between these two cases is that since

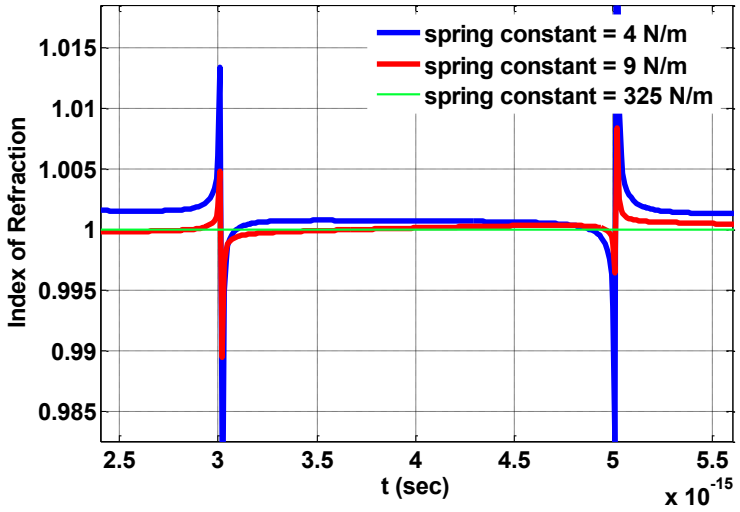

Fig. 2.11. The jump in the time dependent index of refraction where the electric field changes its polarization sign for single Hermitian USCP interaction.

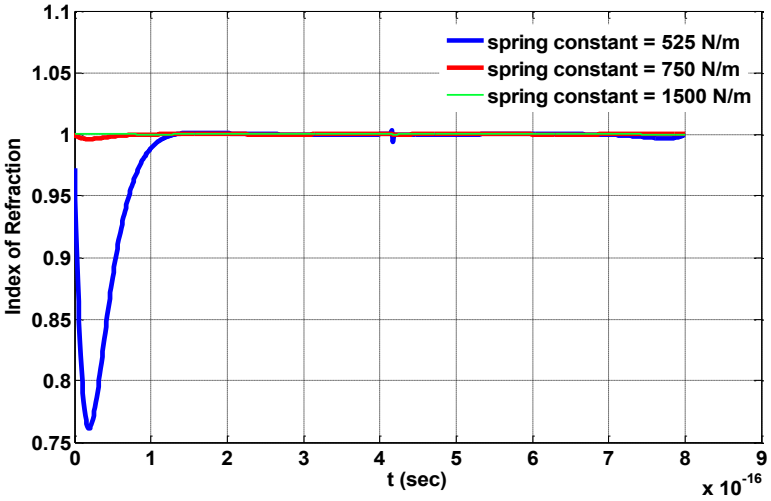

Fig. 2.12. Time dependent index of refraction during the interaction of a single Laguerre USCP with a bound electron without ionization for different spring constant values with a fixed damping constant value ($\gamma_o = 1x10^{16}$ Hz).

there are two points where the Hermitain USCP field changes its polarization sign, we have sudden changes in the perturbation of index of refraction twice around these points. The zoomed view of these regions shows the sudden effects more clearly in Fig 2.11. In Fig. 2.12, we see a similar type of change in the time dependent index of refraction for damping constant $\gamma_o = 1x10^{16}$ Hz.

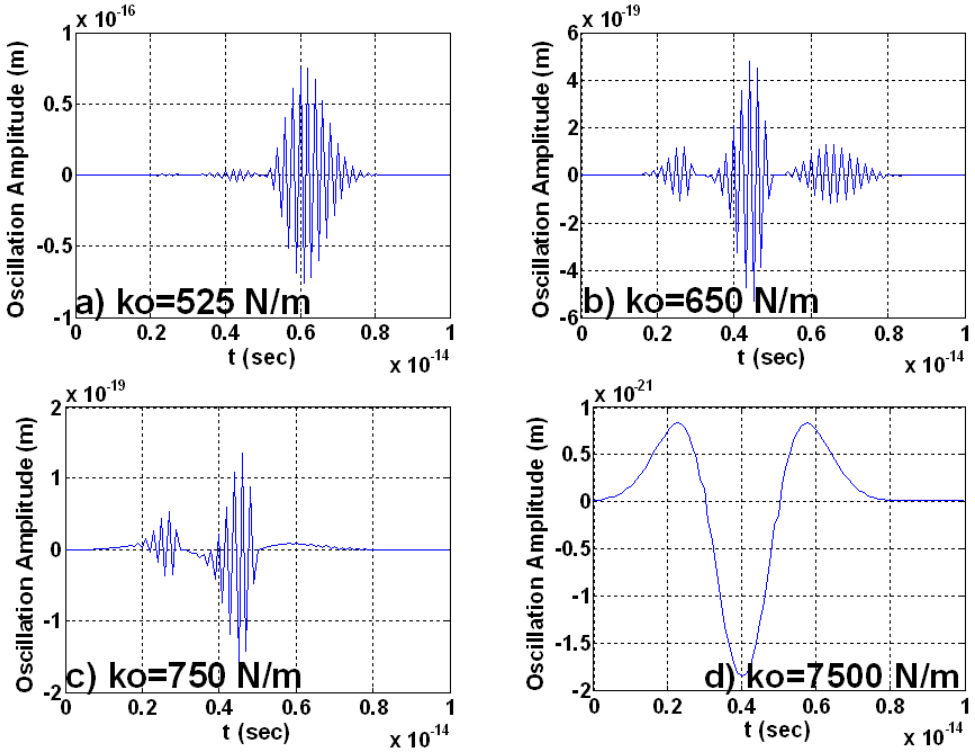

Fig. 2.13. Hermitian pulse excitation oscillations for damping constant: $\gamma_o = 1x10^{17}$ Hz.

For a damping constant value of $1x10^{17}$ (Fig 2.13), very different oscillation behaviors are seen than the previuos cases (Fig. 2.4) of Hermitian pulse excitation. The most prominent feature in Figs. 2.13(a), 2.13(b) and 2.13(c) is the high frequency oscillation profile with a phase delay with respect to excitation pulse. In Fig. 2.13, the spring constant is increased gradually from 2.13(a) to 2.13(c) while keeping the

damping value constant. For a relatively low value of spring constant in Fig. 2.13(a), the main lobe and the trailing tail of the excitation pulse have almost no effect on the oscillation of the electron. The bound electron starts sensing the leading tail of the Hermitian excitation after a phase delay of 5 fs. In Fig. 2.14, the modifier function solutions for the Hermitian pulse excitation for Fig. 2.13 is shown.

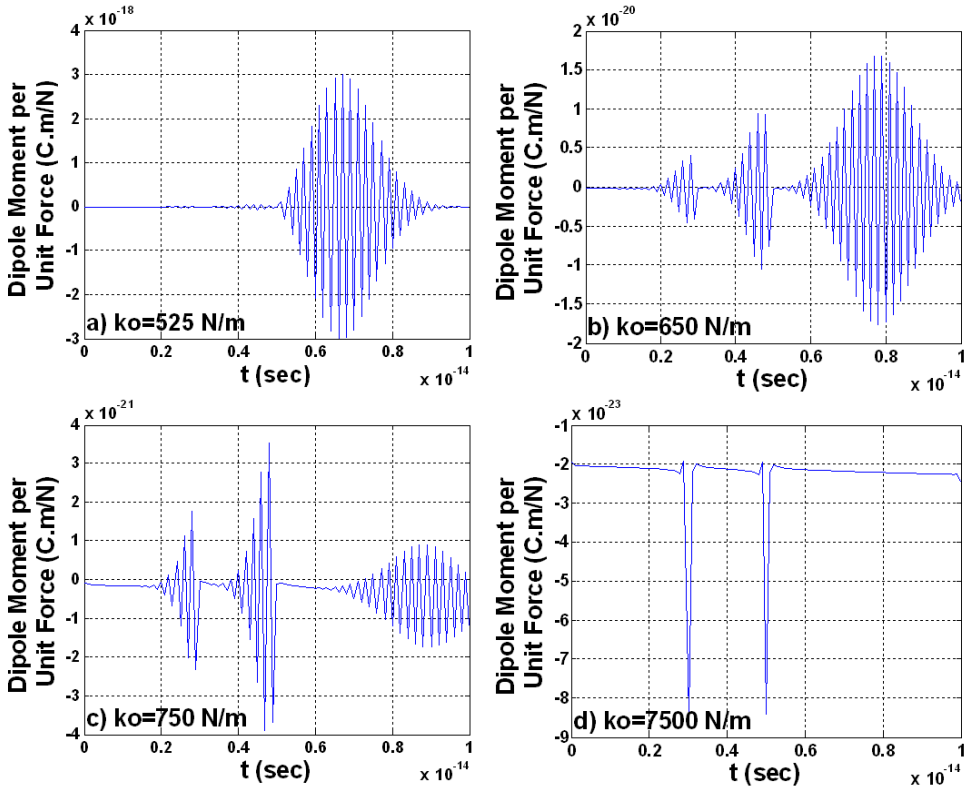

Fig. 2.14. Hermitian pulse excitation modifier functions for damping constant: $\gamma_o = 1x10^{17}$ Hz.

As it is seen in Fig. 2.14(a), modifier function suppresses the interaction effect of main lobe and the trailing tail of Hermitian function. As a result of this, the bound electron starts sensing the excitation pulse with a phase delay [Fig. 2.13(a)] associated with the modifier function. Same behaviour of the modifier function is seen in Figs. 2.14(b) and 2.14(c), too. As a result of this, an approximately 2 fs phase delay occurs in Figs.

2.13(b) and 2.13(c). In Fig. 2.14(d), the type of modifier function is seen that gives a completely phase inverted time profile of the excitation pulse for the oscillation of the bound electron. In Fig. 2.13(d), the stabilized oscillation profile is seen as a result of this modifier function. In Fig. 2.15, as in the Fig. 2.13, there is a high oscillation frequency behaviour in the perturbation effect of the single Hermitian USCP on the index of refraction. Especially, the magnitude of the perturbation effect is more significant around the main lobe and the trailing edge regions than the leading edge region of the applied field. The effect of the Hermitian USCP on the index of refraction decreases as the spring constant increases for the given fixed damping constant value.

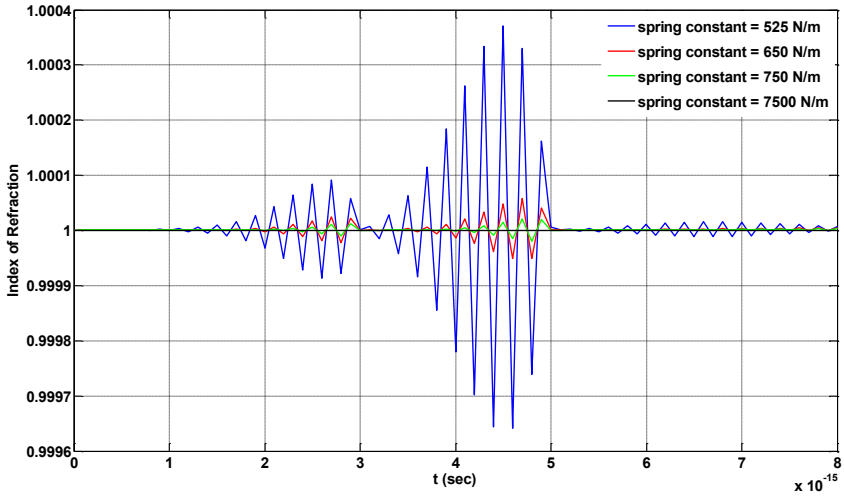

Fig. 2.15. Time dependent index of refraction during the interaction of a single Hermitian USCP with a bound electron without ionization for different spring constant values with a fixed damping constant value ($\gamma_o = 1x10^{17}$ Hz).

CHAPTER 3

CONVOLUTIONAL MODIFIER FUNCTION APPROACH FOR USCP INTERACTION IN TIME DOMAIN WITH A BOUND ELECTRON WITHOUT IONIZATION

3.1 Mathematical Model

In section 2.1, we explained why the oscillation field of the bound electron under single USCP exposure must be defined in terms of the multiplication of the applied USCP with a modifier function. In a more realistic approximation, we need to include a constant updating between the electron motion and the time dependent applied field. This is the major difference between approaches used in sections 2.1 and 3.1. Suppose that we are applying two different USCPs ranging in different spectral content on to the same type of material at different points. If we assume that the majority of the spectral content of one of these USCPs is relatively closer to the natural oscillation frequency of the bound electron of the material than the spectral content of the other USCP (see Fig. 3.1), then it will not be realistic to consider exactly the same type of time domain USCP interaction mechanism (modifier function approach that has been explained in section 2.1) for both of these two different USCPs. As it is seen in Fig. 3.1, we note that since the majority of the spectral content of $USCP_2$ is closer to w_o than the majority of the spectral content of $USCP_1$, in the context of interaction efficiency the interaction of $USCP_2$ will be relatively more intense than the interaction

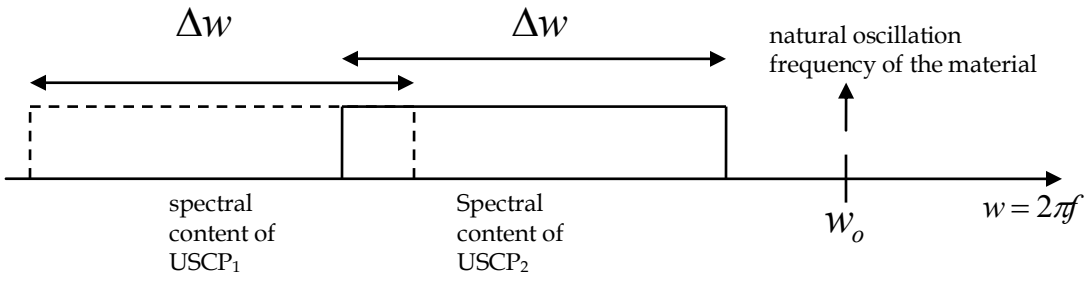

Fig. 3.1. Spectral content of two different USCPs with the same pulse duration. They are being applied to different points on a material which has a natural oscillation frequency of w_o.

of $USCP_1$ for the given spectral content and for the given natural oscillation frequency. Given the formulation provided in section 2.1, we are just directly masking (multiplying) the modifier function (that we found from Eq. 2.14) on to the time domain profile of $USCP_1$ to find the oscillation field of the bound electron during the continuance of this pulse. If we follow the same procedure to calculate the oscillation field of the bound electron under $USCP_2$ excitation, this will cause us to miss the cumulative tendency due to the memory effect of the oscillation field of the bound electron in time domain due to the interaction with single $USCP_2$ compared to the interaction with single $USCP_1$. In order to take into consideration the cumulativeness effect under $USCP_2$ excitation, instead of defining oscillation as in Eq. 2.9, we need to define the time dependent electron motion with a convolution operation since a convolution can be considered as an operation that shows the effect of current and past inputs to the current output of a system:

$$x(t) = x_o(t) * E(t). \tag{3.1}$$

If we plug Eq. (3.1) into Eq. (2.8), we obtain

$$\frac{d^2}{dt^2}\left(x_o(t) * E(t)\right) + \gamma_o \frac{d}{dt}\left(x_o(t) * E(t)\right) + \frac{k_o}{m_e}\left(x_o(t) * E(t)\right) = \frac{q_e}{m_e} E(t). \tag{3.2}$$

Eq. 3.2 allows us to obtain the oscillation field after the pulse (wake-field) due to the nature of convolution operation in Eq. 3.1. The modifier function is a hidden function that must be evaluated first to find the oscillation field caused by the USCP excitation where the source duration is much shorter than the relaxation dynamics of the material. Due to the nature of convolution operation in Eq. 3.1, although the USCP actually vanishes at $t = \tau$ (where τ is the pulse duration), the modifier function will still exist after the end of the pulse and our technique evaluates the oscillation field after the pulse duration due to the memory effect of the convolution operation.

In order to find the modifier function in Eq. 3.2, different mathematical solution techniques can be used. For the work in this chapter, let us use Eq. 3.1 in the following form:

$$f(t) = x_o(t) + x_o(t) * E(t), \tag{3.3 a}$$

$$f(t) = x_o(t) + \int_0^t x_o(t-\tau) E(\tau) d\tau, \tag{3.3 b}$$

which is called Volterra Integral Equation (VIE) of the second kind where the source function $f(t)$ and the kernel function $E(t)$ are given and $x_o(t)$ is the unknown function. There are many existing state of the art numerical techniques for solving the VIE in the literature [82,83,84,85,86,87,88,89]. However, in this chapter we will follow a simpler mathematical procedure in order to obtain physical understanding and insight of differences between convolutional modifier function approach and the modifier function approach explained in section 2.1. Let's define the convolution integral in Eq. 3.3(b) as:

$$\int_0^t x_o(t-\tau)E(\tau)d\tau = f(t)-x_o(t), \tag{3.4}$$

where $f(t)$ is going to be a reasonable trial function that will be defined for finding the modifier function in Eq. 3.2. By plugging the definition in Eq. 3.4 into Eq. 3.2, we obtain:

$$\frac{d^2}{dt^2}x_o(t)+\gamma_o\frac{d}{dt}x_o(t)+\frac{k_o}{m_e}x_o(t)=F(t), \tag{3.5}$$

where

$$F(t)=\frac{d^2}{dt^2}f(t)+\gamma_o\frac{d}{dt}f(t)+\frac{k_o}{m_e}f(t)-\frac{q_e}{m_e}E(t). \tag{3.6}$$

While in Eq. 2.14 in section 2.1 we are calculating the modifier function for time dependent damping and spring coefficients, in Eq. 3.5 we calculate the modifier function for constant damping and spring coefficients with a time dependent source term modified by the trial function $f(t)$. This approach allows us to incorporate the cumulative tendency of the oscillation field and memory effect originating from the spectral content of the USCP and to have constant damping and spring coefficients during the pulse continuance.

3.2 Numerical Results and Discussions

For our numerical calculations, we used the following forms as two trial functions simultaneously for the Laguerre USCP excitation case:

$$f_1(t) = f_{o1}\left(\exp\left(-\beta^2\right) - Sin\left(\beta^a\right)\right), \tag{3.7}$$

$$f_2(t) = f_{o2}\left(\exp\left(-\beta^2\right) + Sin\left(\beta^a\right)\right), \tag{3.8}$$

where $\beta = t - zc^{-1}/to$. a can range from 1 to m according to the chosen $f(t)$. So, at the end of the calculations, the total oscillation field has been evaluated as:

$$x(t) = \frac{1}{2m}\sum_{i=1}^{m}\left[x_{o1i}(t) * E(t) + x_{o2i}(t) * E(t)\right] \tag{3.9}$$

where $x_{o1i}(t)$ is calculated for $f_1(t)_{a=i}$ and $x_{o2i}(t)$ is calculated for $f_2(t)_{a=i}$ from Eq. 3.5.

For the Hermitian USCP excitation case, we used the following form as the trial function in the numerical calculations:

$$f_3(t) = f_{o3}\left(1 - \beta^{-a}\right) \tag{3.10}$$

and the total oscillation field has been evaluated as:

$$x(t) = \frac{1}{m}\sum_{i=1}^{m}\left[x_{o3i}(t) * E(t)\right] \tag{3.11}$$

where $x_{o3i}(t)$ is calculated for $f_3(t)_{a=i}$ from Eq. 3.5.

The values of the amplitude constants f_{o1}, f_{o2}, and f_{o3} are dependent on the trial functions and the number of trial functions that are chosen for the solution of the modifier function.

In Fig. 3.2, we see some important results of the convolutional modifier function approach on the oscillation field of the bound electron under Laguerre and Hermitian USCP excitation and both have close spectral content to the natural oscillation frequency of the material. Although there is not much difference in the oscillation frequency compared to the Fig. 2.4 in section 2.2, there is a significant difference in the oscillation amplitude where the convolutional modifier function approach has higher amplitudes. In addition to this (different than Fig. 2.4), in Fig. 3.2 we see some phase delay in the oscillation field with respect to the applied USCP for both Laguerre and Hermitian excitations (see Figs. 3.2(a), 3.2(b), 3.2(c), 3.2(e), 3.2(g), 3.2(h), 3.2(i)

and 3.2(j)). Another significant result shown in Fig. 3.2, due to the nature of the convolution operation, we can see the oscillation in the wake-field after the continuance of the USCP.

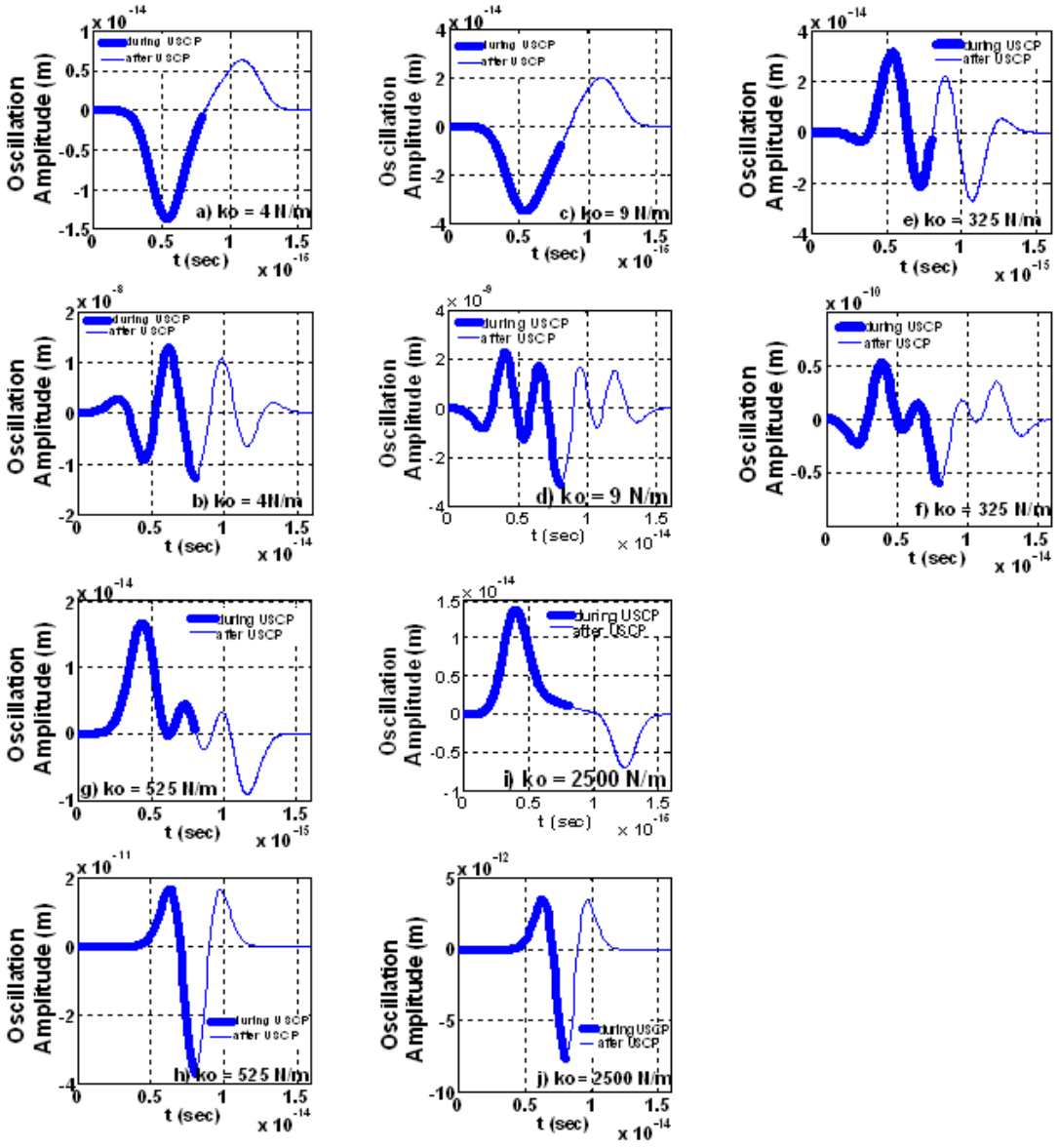

Fig. 3.2. Bounded electron motion for the convolutional modifier function approach under Laguerre USCP excitation ((a), (c), (e), (g), (i)) and Hermitian USCP excitation ((b), (d), (f), (h), (j)) for various values of spring constant (k_o) with a fixed damping constant ($\gamma_o = 1x10^{14}$ Hz).

For Fig. 3.3, we have higher oscillation amplitude and almost the same oscillation frequency as compared to Fig. 2.5. Also in Figs. 3.3(a), 3.3(b) and 3.3(c) there is a phase delay which is not seen in Figs. 2.5(a) and 2.5(b). It is observed that comparing Fig. 3.2 to Fig. 3.3, there is a significant difference in the wake-field oscillations which are attenuated much quicker in Fig. 3.3 after the end of the pulse continuance.

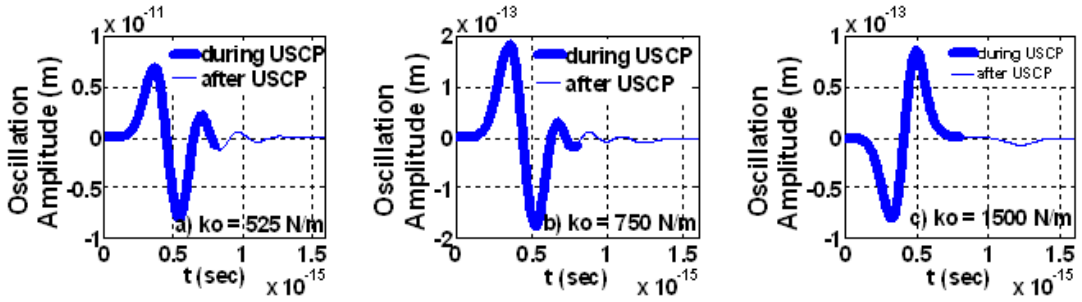

Fig. 3.3. Bounded electron motion for the convolutional modifier function approach under Laguerre USCP excitation for various values of spring constant (k_o) with a fixed damping constant ($\gamma_o = 1x10^{16}$ Hz).

In Figs. 3.4 and 3.5, real and imaginary part of the perturbation effect of an applied single Laguerre USCP on the index of refraction of the given $k_o - \gamma_o$ medium. is shown for the convolutional modifier function approach. The common behavior that we note in Figs. 2.8, 3.4 and 3.5 is that there is a sudden jump for real and imaginary parts of the index of refraction at the point where the USCP field changes its polarization sign. Another point that we must note in Figs 3.4 and 3.5 is that, when the real part of the perturbation effect vanishes at some regions of the Laguerre USCP, the imaginary part of the perturbation effect on the index of refraction comes into play.

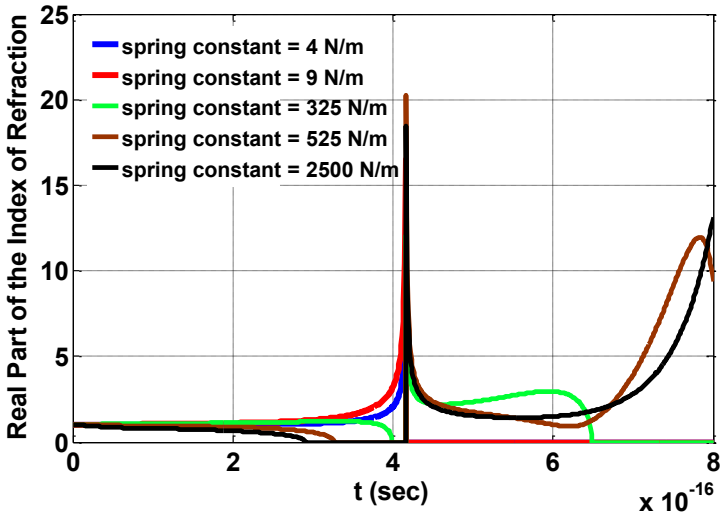

Fig. 3.4. Real part of the time dependent index of refraction during the interaction of a single Laguerre USCP with a bound electron without ionization for different spring constant values with a fixed damping constant ($\gamma_o = 1x10^{14}$ Hz) [see Eq. 2.6].

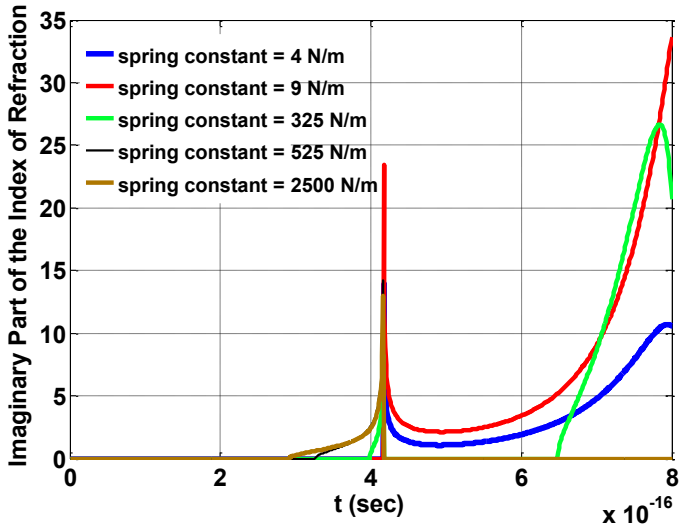

Fig. 3.5. Imaginary part of the time dependent index of refraction during the interaction of a single Laguerre USCP with a bound electron without ionization for different spring constant values with a fixed damping constant ($\gamma_o = 1x10^{14}$ Hz) [see Eq. 2.6].

3.3 Numerical solution of Volterra integral equation

Once the oscillation field of the bound electron is defined as in Eq. (3.1), VIE of the second kind has been utilized in Eq. (3.3b) to find a solution for the modifier function $x_o(t)$. Due to the commutative property of convolution operation, we can write Eq. (3.3b) as:

$$f(t) = x_o(t) + \int_0^t E(t,\tau) x_o(\tau) d\tau, \quad 0 \le t \le 1, \tag{3.12}$$

where $E(t,\tau)$ is the applied USCP as the convolutional kernel and $f(t)$ is a given source function. For a general VIE of the second kind with a convolutional kernel, the approximate closed form solution can be evaluated by using the Modified Taylor-series expansion method which is defined in [82]. This method can be applied to a wide class of VIEs of the second kind with smooth and weakly singular kernels and it gives an approximate and explicit closed form solution which can be computed using symbolic computing codes [82]. Due to the smoothness of the kernel $E(t,\tau)$, only few terms in the Taylor expansion are enough to get high accuracy [82]. In this work, we apply Taylor expansion up to the second order. So, if we apply the procedure explained in [82] onto Eq. (3.12), we obtain the following equations :

$$f(t) = \left[1 + \int_0^t E(t,\tau) d\tau\right] x_o(t) + \left[\int_0^t E(t,\tau)(\tau - t) d\tau\right] x_o'(t) + \left[\frac{1}{2}\int_0^t E(t,\tau)(\tau - t)^2 d\tau\right] x_o''(t), \tag{3.13}$$

$$f'(t) = x_o'(t) + \left[E(t,t) + \int_0^t \frac{\partial E(t,\tau)}{\partial t} d\tau \right] x_o(t), \tag{3.14}$$

$$f''(t) = x_o''(t) + E(t,t)x_o'(t) + \left[2\frac{\partial E(t,t)}{\partial t} + \int_0^t \frac{\partial^2 E(t,\tau)}{\partial t^2} d\tau \right] x_o(t), \tag{3.15}$$

where $x_o'(t)$ and $f'(t)$ are the 1st derivative, $x_o''(t)$ and $f''(t)$ are 2nd derivative of these terms with respect to time. Here, our aim is to find $x_o(t)$, using Eqs. (3.13), (3.14) and (3.15). Performing the necessary manipulation, we obtain the explicit definition of $x_o(t)$ as:

$$x_o(t) = \frac{f(t) - f'(t)I_2(t) - \frac{1}{2}f''(t)I_3(t) + \frac{1}{2}E(t,t)f'(t)I_3(t)}{1 + I_1(t) - I_2(t)[E(t,t) + I_4(t)] + \frac{1}{2}E^2(t,t)I_3(t) + \frac{1}{2}E(t,t)I_3(t)I_4(t) - \frac{1}{2}I_3(t)I_5(t)}, \tag{3.16}$$

where $I_1(t) = \int_0^t E(t,\tau)d\tau$, $I_2(t) = \int_0^t E(t,\tau)(\tau - t)d\tau$, $I_3(t) = \int_0^t E(t,\tau)(\tau - t)^2 d\tau$, $I_4(t) = \int_0^t \frac{\partial E(t,\tau)}{\partial t} d\tau$ and $I_5(t) = \int_0^t \frac{\partial^2 E(t,\tau)}{\partial t^2} d\tau$. Here, $E(t,\tau) = E(t-\tau)$ and $E(t,t) = E(t,\tau = t)$. For Laguerre USCP:

$$E(t,\tau)=\exp\left(-\left(7.5\left(\frac{t-\tau}{t_o}-0.4167\right)\right)^2\right)\left[-\frac{1}{24}\left(\frac{t-\tau}{t_o}-0.4167\right)^4+\frac{15}{24}\left(\frac{t-\tau}{t_o}-0.4167\right)^3-\frac{5}{2}\left(\frac{t-\tau}{t_o}-0.4167\right)^2+2\left(\frac{t-\tau}{t_o}-0.4167\right)\right].$$

(3.17)

From Eq. (3.17), $E(t,\tau=t)=-7.5293x10^{-5}$ is found for Laguerre USCP. For Hermitian USCP:

$$E(t,\tau)=\left(1-\left(\frac{t-\tau}{t_o}-4.0167\right)^2\right)\exp\left(-\left(\frac{t-\tau}{t_o}-4.0167\right)^2/2\right). \quad (3.18)$$

From Eq. (3.18), $E(t,\tau=t)=-0.0047$ is found for Hermitian USCP. Eqs. (3.17) and (3.18) are going to be used in Eq. (3.16) separately for Laguerre and Hermitian USCP excitation cases. We also need to define $f(t)$ in Eq. (3.16) which is apriori given term in a VIE solution of the second kind (Eq. (3.12)). In this section, we will use the same $f(t)$ functions that have been used in section3.1. From Eqs. (3.7) and (3.8), we will obtain two different VIE solutions, $x_{o1}(t)$ and $x_{o2}(t)$. Using these two solutions, we will define the final VIE solution for the modifier function as:

$$x_{oV}(t)=\frac{x_{o1}(t)+x_{o2}(t)}{2}. \quad (3.19)$$

We now have the explicit solution of the modifier function. But this solution is not coupled with the physical parameters of the problem such as spring and damping constants. In order to do this, we will go back to the procedure used in section 3.1 and we will use $x_{oV}(t)$ in the procedure of convolutional modifier function approach for the solution of Lorentz damped oscillator model. This time, instead of finding a modifier function, we will find a new $f(t)$ function and then we will use this function in Eq. (3.16) to find the desired modifier function which has already been coupled with the physical parameters of the problem. So, if we plug $x_{oV}(t)$ into:

$$\frac{d^2}{dt^2}x_{oV}(t)+\gamma_o\frac{d}{dt}x_{oV}(t)+\frac{k_o}{m_e}x_{oV}(t)=F(t). \tag{3.20}$$

Once we find $F(t)$ explicitly in Eq. (20), we can use it in:

$$\frac{d^2}{dt^2}f_V(t)+\gamma_o\frac{d}{dt}f_V(t)+\frac{k_o}{m_e}f_V(t)=F(t)+\frac{q_e}{m_e}E(t), \tag{3.21}$$

where $E(t)$ is the applied USCP and $f_V(t)$ is the function that we are going to use it in Eq. (3.16) for the VIE solution of the modifier function. Eqs. (3.20) and (3.21) are directly obtained from section 3.1 (see Eqs. 3.5 and 3.6). The summary of the procedure is shown below in Fig. 3.6. Same roadmap has been followed for the Hermitian USCP excitation where Eq. 3.10 is used for the initial $f(t)$ function.

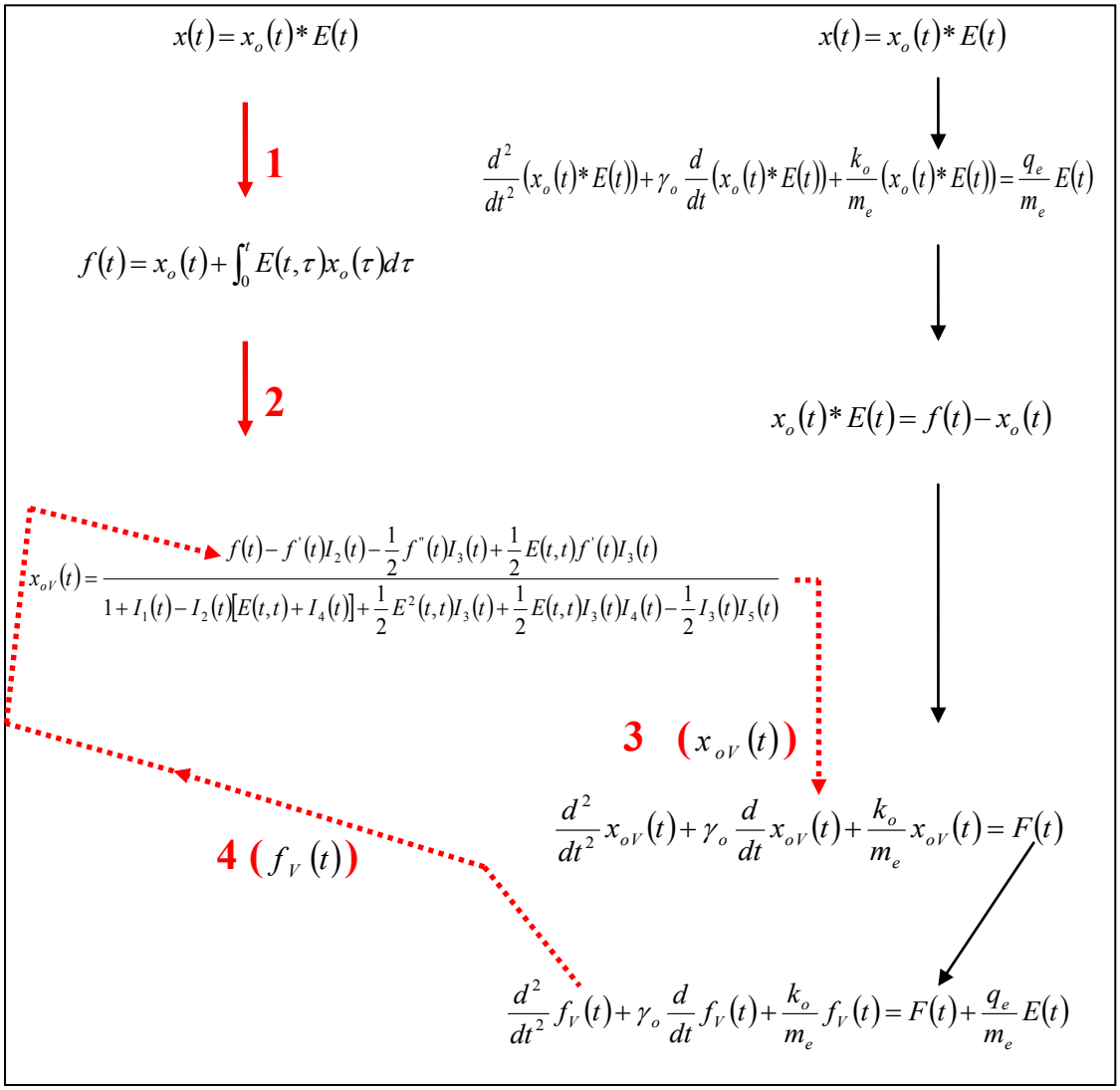

Fig. 3.6. Roadmap used in this section. The flow on the right with dark arrows is the procedure used in section 3.1.

Once we find the modifier function, we can define the oscillation field explicitly under USCP excitation [see Eq. (3.1)]. This will provide us to see clearly the change of the index of refraction in time domain in the period of one USCP duration via Eq. 2.6. where $P_{pol}(t)$ is the electronic polarization which is defined as $P_{pol}(t)=Nq_e x(t)$. Here, N is the number of electrons taken into consideration per unit volume for the

interaction process. In this section, in order to understand the perturbation effect of the applied USCP on the change of the index of refraction of the medium in one pulse duration better, we will use the normalized form of Eq. (2.6). This will provide us to see the time evolution picture of the refractive index in one USCP duration in a sense of free from the electron density effect of the environment.

3.4 Numerical results and discussions for VIE solution

Fig. 3.7 shows the VIE solution of the convolutional modifier function approach for the motion of a bounded electron under Laguerre USCP excitation [see Figs. 3.7(a), 3.7(c), 3.7(e), 3.7(g) and 3.7(i)] and Hermitian USCP excitation [see Figs. 3.7(b), 3.7(d), 3.7(f), 3.7(h) and 3.7(j)] for various values of spring constant with a fixed value of damping constant. The arrow on the oscillation graphs indicate the time where the duration of the applied USCP field ends. Due to the nature of convolution operation, we can monitor the oscillation field of the bound electron up to 2τ where τ is the actual duration of the USCP. We use exactly the same spring constant values for the same fixed damping constant value used in the previous sections. Although it is not very dramatic, there are some differences between the results of this section and section 3.2. These differences are not only seen in the amplitude of the oscillation fields but also seen in the characteristics of the time profile. The major difference for Laguerre excitation is seen for the relatively higher values of the spring constant. In Fig. 3.7(g), comparing to the oscillation field in Fig. 3.2(g), which has the same physical parameters used for Fig. 3.7(g), we see a relatively higher oscillation amplitudes in the second half cycle of the USCP and in the late oscillation region just

after the USCP. In Fig. 3.7(i), the difference is more dramatic comparing to the oscillation in Fig. 3.2(i). While we see almost exactly the same type of half cycle

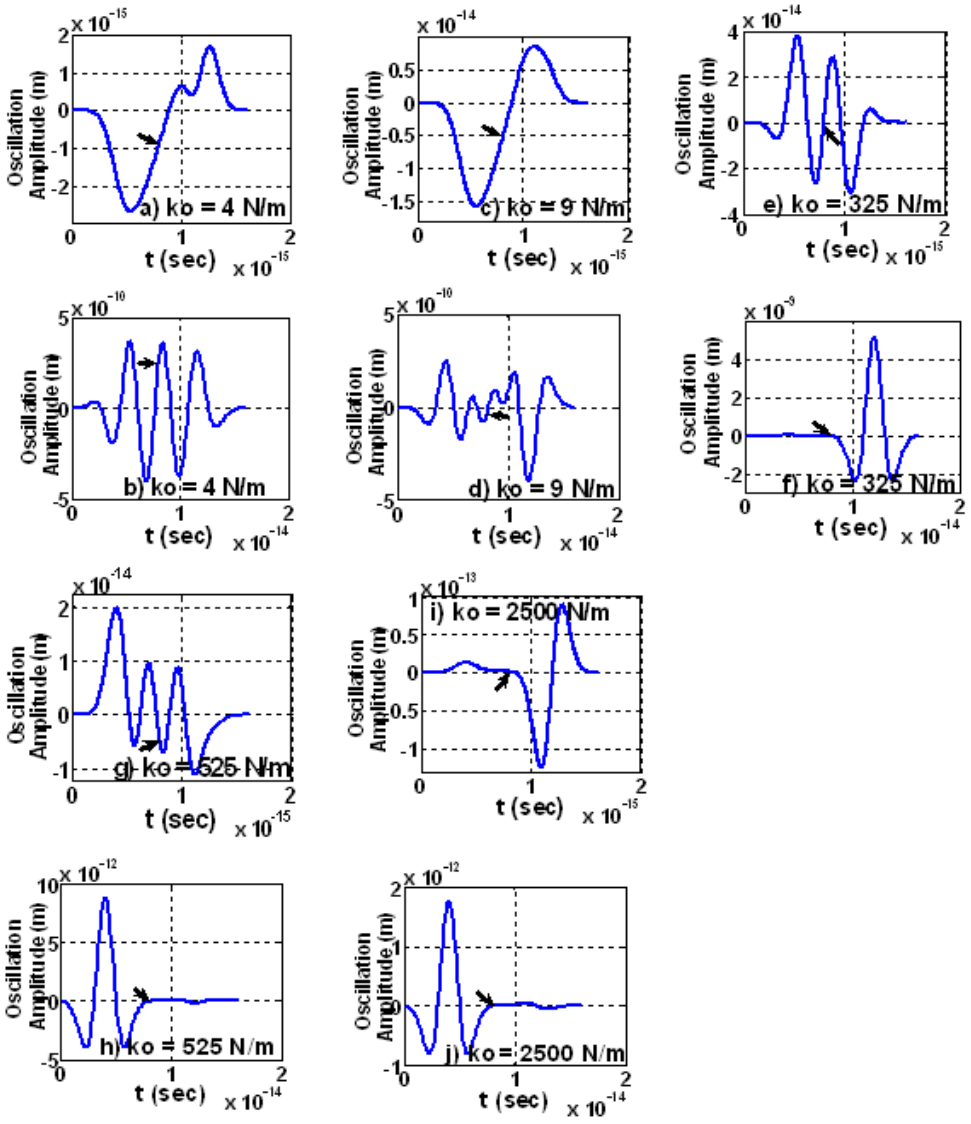

Fig. 3.7. Bounded electron motion for the Volterra integral equation solution of the convolutional modifier function approach under Laguerre USCP excitation ((a), (c), (e), (g), (i)) and Hermitian USCP excitation ((b), (d), (f), (h), (j)) for various values of spring constant (k_o) with a fixed damping constant ($\gamma_o = 1x10^{14} Hz$). (Arrangement of the graphs allow one to compare early $(0-\tau_p)$ and late $(\tau_p - 2\tau_p)$ oscillations).

oscillation in the whole period of the pulse duration in both Figs. 3.7(i) and 3.2(i) with closely the same peak value, the late oscillation behavior, which is the oscillation after the interaction with the applied USCP, is completely different. As a late oscillation behavior, we see the inverted phase profile of the applied Laguerre USCP between the duration of τ_p and $2\tau_p$ period. For the higher spring constant values with the same fixed damping constant, oscillation behavior settles down into this time profile between 0 and $2\tau_p$ period seen in Fig. 3.7(i). For the Hermitian interaction, we see more dramatic differences between the Figs 3.7 and 3.2. Especially for the relatively high spring constant values, time phase delay behavior shows important deviation between two figures. In Fig. 3.7(f), we have almost one τ_p phase delay before the occurrence of the oscillation while there is no phase delay in Fig. 3.2(f). On the other hand, in Figs. 3.7(h) and 3.7(j), different than the oscillations in Figs. 3.2(h) and 3.2(j), we do not see any inverted time phase profile of the applied USCP and any time phase delay in the oscillation behavior. For the higher spring constant values, the oscillation behavior settles down into this time profile.

Fig. 3.8 shows the normalized value of the change of the refractive index of the given $k_o - \gamma_o$ medium in the interaction duration of the applied Laguerre USCP. As it is shown in Eq. (2.6), the number of electrons in the unit volume of the material contributing to the polarization will effect the change in the index of refraction. But more than the contribution of the bound electron population, we are interested in the effect of the oscillation response of each single electron on the refractive index under a single USCP excitation. So, different than section 3.2, since it is more intuitive, in this section we have a normalized picture of the process in order to understand the pure

perturbation effect of the applied USCP – bound electron interaction on the time evolution of the refractive index of the medium. For example, if we look at to Fig. 3.8(a), around the close proximity of $7x10^{-16}$ second, it is seen that the perturbation effect of the applied USCP on the real part of the refractive index is two times stronger for the medium with $k_o = 525N/m$ than for the medium $k_o = 2500N/m$. As an other example, for the material $k_o = 325N/m$ in Fig. 3.8(a), it is seen that the perturbation effect of the Laguerre USCP is approximately four times higher around

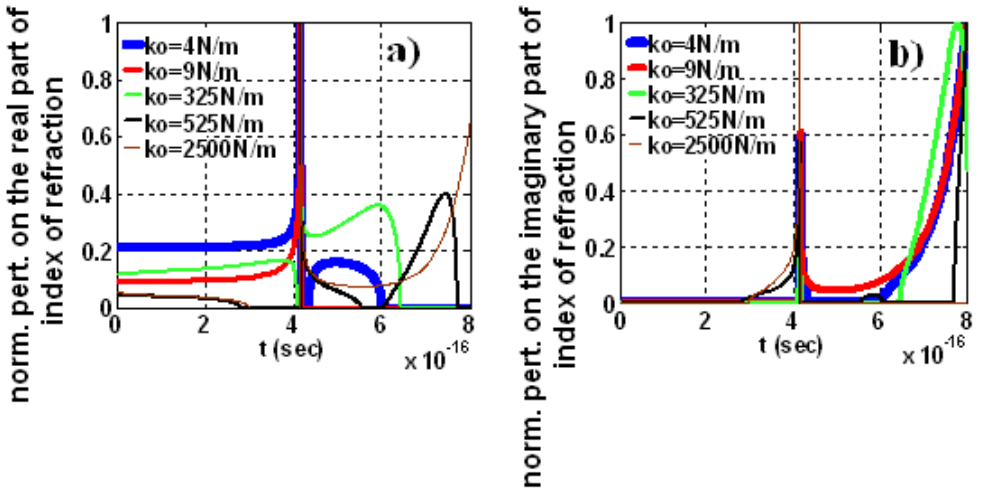

Fig. 3.8. Normalized real part perturbation **(a)** and normalized imaginary part perturbation **(b)** of the time dependent index of refraction during the interaction of a single Laguerre USCP with a bound electron without ionization for different spring constant values with a fixed damping constant ($\gamma_o = 1x10^{14}$ Hz).

the proximity of $6x10^{-16}$ second than the perturbation effect occurred around the proximity of $2x10^{-16}$ second for the same material. In Fig. 3.8(b), it is clearly seen that there are different increment and decrement ratios at the different parts of the pulse duration for the imaginary part as it is seen in the real part. Thus, the

real and imaginary parts of the index of refraction are variable during the pulse duration.

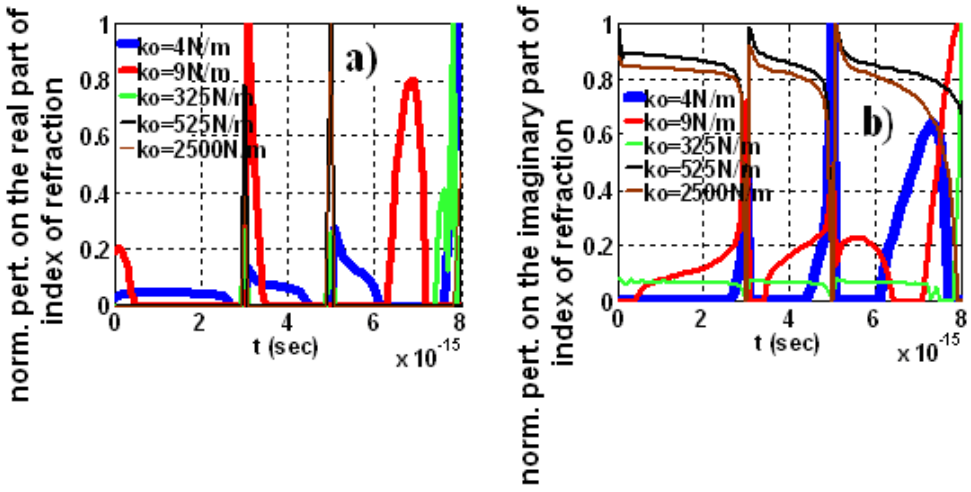

Fig. 3.9. Normalized real part perturbation **(a)** and normalized imaginary part perturbation **(b)** of the time dependent index of refraction during the interaction of a single Hermitian USCP with a bound electron without ionization for different spring constant values with a fixed damping constant ($\gamma_o = 1x10^{14}$Hz).

Fig. 3.9 shows the same normalized effects that are being discussed for Fig. 3.8, but this time it is for Hermitian USCP excitation case. As it is seen clearly in Figs 3.9(a) and 3.9(b), the normalized perturbation effects are too different than the Laguerre excitation case in Figs. 3.8(a) and 3.8(b). For Hermitian case, we see sharper increments and decrements in the perturbations both for the real and imaginary parts.

A common and an important feature seen (we see the same type of behavior in section 3.2, too) in both of the Figs. 3.8 and 3.9 is that, while there is a change in the real part at some specific part of the applied USCP, the imaginary part is completely suppressed for both Laguerre and Hermitian excitation cases. The vice versa of this

effect is also seen, i.e., while there is a change in the imaginary part at some specific part of the applied USCP, the real part is completely suppressed. So, we can say that there are some subdurations where only the real part of the index of refraction is dominant and at the rest of the subdurations only the imaginary part of the index of refraction is dominant in the duration of a single USCP. This outcome is very promising and might be very important for some applications such as pump-probe experiments, enhanced imaging resolution, optical lithography and refractive index control [90,91,92,93]. The simultaneous occurrence of real and imaginary parts are seen only as a sudden jump at the crossover points of the USCPs. In order to show this behavior more clearly, Figs. 3.8(a) and 3.8(b) are plotted separately in Fig. 3.10 and Figs. 3.9(a) and 3.9(b) are plotted separately in Fig. 3.11.

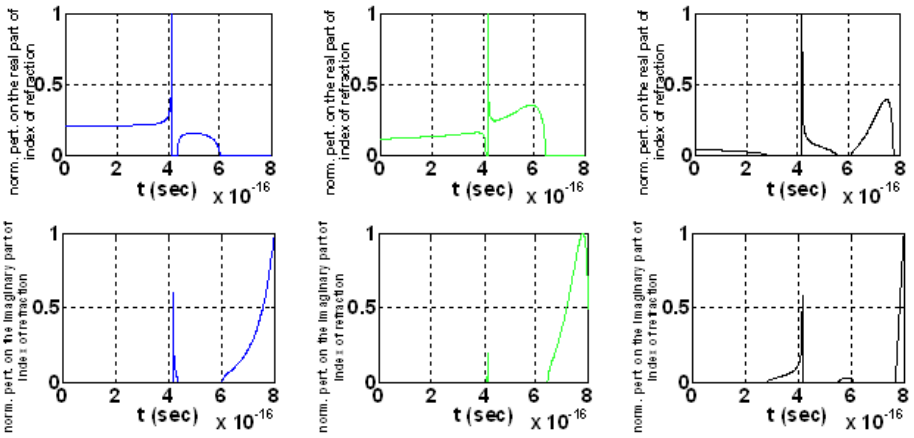

Fig. 3.10 Separate plotting of Fig. 3.8(a) (upper row: real part perturbation), and Fig. 3.8(b) (lower row: imaginary part perturbation) for $k_o = 4N/m$, $k_o = 325N/m$ and $k_o = 525N/m$. Colors correspond to same values of the legend in Fig. 3.8.

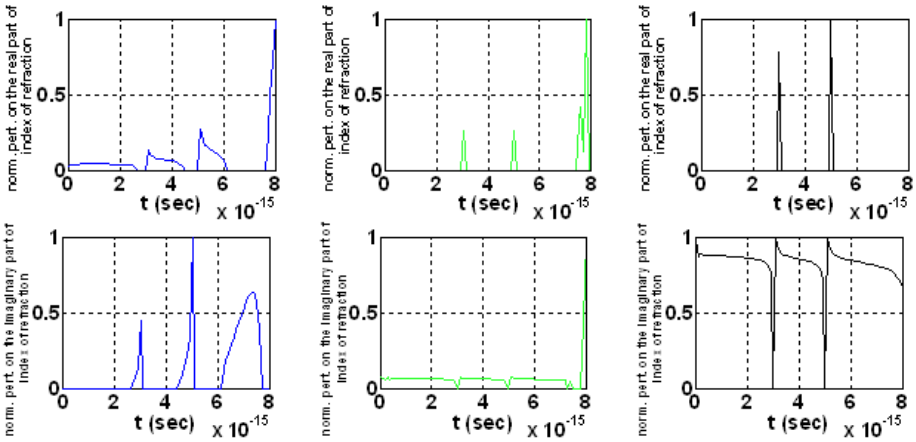

Fig. 3.11. Separate plotting of Fig. 3.9(a) (upper row: real part perturbation), and Fig. 3.9(b) (lower row: imaginary part perturbation) for $k_o = 4N/m$, $k_o = 325N/m$ and $k_o = 525N/m$. Colors correspond to same values of the legend in Fig. 3.9.

CHAPTER 4

CONCLUSIONS

The results of this work indicate that if the applied field is a USCP, then it is not possible to separate the field into pieces to find the polarization effect of each part of the applied field on a bound electron since the USCP can not be further broken down into separate pieces of the applied field. The traditional Fourier method of multiplying the Delta function response with the applied field and integrating (superposing) this product in time can only be used for slowly varying envelope approximation which is not realistic for single cycle pulses of unity femtosecond and attosecond applied fields. In a USCP case, the Lorentz oscillator model must be modified in order to find the polarization effect of a single USCP. Since a USCP is extremely broadband, it is not realistic to use a center frequency in the calculations as is done in the Fourier series expansion approach. Results in this work are presented on the transient response of the system during the USCP duration without switching to frequency domain. In order to accomplish this mathematically, we developed a new technique we label as the "Modifier Function Approach". The modifier function is embedded in the classic Lorentz damped oscillator model and by this way, we upgrade the oscillator model so that it is compatible with the USCP on its right side as the driving force. Results of this work also provide a new modified version of the Lorentz oscillator model for ultrafast optics. The results also indicate that the time response of the two models used

to represent the USCP can alter the time dependent polarization of the material as it interacts with a single cycle pulse.

As a second model, that we label as the "Convolutional Modifier Function (CMF) Approach", we chose to provide a convolution of the applied field and the embedded modifier function for a further refinement of the classical Lorentz damped oscillator model. This technique is proposed for the interaction of a USCP with a bound electron in a close resonance case. The convolution approach allows one to incorporate previous motion of the electron with the interacting applied field. Results are compared for the motion of the electron for each case and the observed change in the index of refraction as a function of time for two different cases. As expected, the index of refraction is not a constant in the ultra short time time domain under the assumptions applied in these studies. The motion of the electron is also highly dependent on the type of input single cycle pulse applied (Laguerre or Hermitian).

We also extended the second model in section 3.3 by employing the modified Taylor series expansion method for the solution of VIE in CMF technique. The extended work shows both some common results and different results when compared to the results of the first version of CMF approach in Section 3.1. The most important result illustrated by the current work is that, during the interaction of a USCP with a bound electron, there are some time durations of the USCP where only the real part or only the imaginary part of the index of refraction exists. This will have important consequences in the interaction dynamics. The current work sheds light on the meaning of the complex index of refraction during the interaction of a USCP both during and after the pulse ends.

REFERENCES

[1] G. Steinmeyer, D. H. Sutter, L. Gallmann, N. Matuschek, and U. Keller, "Frontiers in Ultrashort Pulse Generation: Pushing the Limits in Linear and Nonlinear Optics," *Science* 286 (5444), 1507-1512, 1999.

[2] M. Y. Shverdin, D. R. Walker, S. N. Goda, G. Y. Yin, and S. E. Harris, "Breaking the single-cycle barrier," Photonics Spectra, 92-105, February 2005.

[3] A. V. Sokolov, "Single-cycle optical pulses synchronized with molecular oscillations," *Appl. Physics B* 77, 343-347, 2003.

[4] G. Krauss, S. Lohss, T. Hanke, A. Sell, S. Eggert, R. Huber, and A. Leitenstorfer, "Synthesis of a single cycle of light with compact erbium-doped fibre technology," *Nature Photonics* 4, 33-36, 2010.

[5] S. Rausch, T. Binhammer, A. Harth, J. Kim, R. Ell, F. X. Kartner, and U. Morgner, "Controlled waveforms on the single-cycle scale from a femtosecond oscillator," Optics Express, Vol. 16, No. 13, 9739-9745, 2008.

[6] S. Sartania, Z. Cheng, M. Lenzner, G. Tempea, Ch. Spielmann, F. Krausz, and K. Ferencz, "Generation of 0.1 TW 5 fs optical pulses at a 1 kHz repetition rate," Opt. Lett. Vol. 22, No. 20, 1997

[7] B. Schenkel, J. Biegert, U. Keller, C. Vozzi, M. Nisoli, G. Sansone, S. Stagira, S. De Silvestri, and O. Svelto, "Generation of 3.8 fs pulses from adaptive compression of a cascaded hollow fiber supercontinuum,' Opt. Lett, Vol. 28, No. 20, 1987-1989, 2003.

[8] G. M. Gale, M. Cavallari, T. J. Driscoll, and F. Hache, "Sub-20-fs tunable pulses in the visible from an 82-MHz optical parametric oscillator, "Opt. Lett, Vol. 20, 1562-1564, 1995.

[9] T. Wilmhelm, J. Paul, and E. Riedle, "Sub-20-fs pulses tunable across the visible from a blue-pumped single-pass noncollinear parametric converter," Opt. Lett, Vol. 22, 1494-1496, 1997.

[10] A. Baltuska, T. Fuji, and T. Kobayashi, "Visible pulse compression to 4 fs by optical parametric amplification and programmable dispersion control," Opt. Lett, Vol. 27, 306-308, 2002.

[11] D. Brida, G. Cirmi, C. Manzoni, S. Bonora, P. Villoresi, S. De Silvestri, and G. Cerullo, "Sub-two-cycle light pulses at 1.6 μm from an optical parametric amplifier," Opt. Lett, Vol. 33, 741-743, 2008.

[12] S. Rausch, T. Binhammer, A. Harth, F. X. Kartner, and U. Morgner, "Few-cycle femtosecond field synthesizer," Opt. Express, Vol. 16, 17410-17419, 2008.

[13] F. Krausz, "From femtochemistry to attophysics," Physics World, ISSN: 0953-8585, 41-46, September 2001.

[14] U. Morgner, "Single-cycle pulse generation," Nature Photonics, Vol. 4, January 2010.

[15] V. Tosa, K. Kovacs, C. Altucci, and R. Velotta, "Generating single attosecond pulse using multi-cycle lasers in a polarization gate," Optics Express, Vol. 17, No. 20, 17700-17710, 2009.

[16] A. Couairon, H. S. Chakraborty, and M. B. Gaarde, "From single-cycle self-compressed filaments to isolated attosecond pulses in noble gases," *Physical Review* A 77, 053814, 2008.

[17] F. Krausz, and M. Ivanov, "Attosecond physics," Review of Modern Physics, Vol. 81, 263-234, 2009.

[18] H. Teng, C. Yun, H. Han, J. Zhu, X. Zhong, W. Zhang, Q. Du, W. Zhang, Z. Wei, "Carrier-envelope phase stabilized 5 fs laser and generation of continuum XUV radiation," CLEO, Pacific Rim, Shanghai, China, 2009.

[19] E. Goulielmakis, M. Schultze, M. Hofstetter, V. S. Yakovlev, J. Gagnon, M. Uiberacker, A. L. Aquila, E. M. Gullikson, D. T. Attwood, R. Kienberger, F. Krausz, and U. Kleineberg, "Single-Cycle Nonlinear Optics," *Science* Vol. 320, 1614-1617, 2008.

[20] P. B. Corkum and F. Krausz, "Attosecond science," *Nature Physics* 3, 381-387, 2007.

[21] A. Baltuska, T. Udem, M. Ulberacker, M. Hentschel, E. Goullelmakis, C. Gohle, R. Holzwarth, V. S. Yakovlev, A. Scrinzi, T. W. Hansch, and F. Krausz, "Attosecond control of electronic processes by intense light fields," Nature, Vol. 421, 611-615, 2003.

[22] H. Niikura, F. Legare, R. Hasbani, A.D. Bandrauk, M.Y. Ivanov, D.V. Villeneuve, and P. B. Corkum, "Sub-laser-cycle electron pulses for probing molecular dynamics," *Nature* 417, 917–922, 2002.

[23] A. Couairon, J. Biegert, C. P. Hauri, W. Kornelis, F. W. Helbing, U. Keller, and A. Mysyrowicz, "Self-compression of ultrashort laser pulses down to one

optical cycle by filamentation," *Journal of Modern Optics*, Vol. 53, No. 1-2, January 2006.

[24] M. Y. Shverdin, D. R. Walker, D. D. Yavuz, G. Y. Yin, and S. E. Harris, "Generation of a Single-Cycle Optical Pulse," Phys. Rev. Lett., Vol. 94, 033904, 2005.

[25] A. V. Sokolov, and S. E. Harris, "Ultrashort pulse generation by molecular modulation," J. Opt. B:Quantum Semiclass. Opt., Vol. 5, R1-R26, 2003.

[26] S.E. Harris, and A. V. Sokolov, "Broadband spectral generation with refractive index control," Phys. Rev. A, Vol. 55, No. 6, 4019-4022, 1997.

[27] D. D. Yavuz, D. R. Walker, G. Y. Yin, and S. E. Harris, "Rotational Raman generation with near-unity conversion efficiency," Opt. Lett., Vol. 27, No. 9, 769-771, 2002.

[28] S. E. Harris, and A. V. Sokolov, "Subfemtosecond Pulse Generation by Molecular Modulation," Phys. Rev. Lett., Vol. 81, No. 14, 2894-2897, 1998.

[29] A. V. Sokolov, D. D. Yavuz, and S. E. Harris, "Subfemtosecond pulse generation by rotational molecular modulation," Opt. Lett. Vol. 24, No. 8, 557-559, 1999.

[30] A. V. Sokolov, "Subfemtosecond compression of periodic laser pulses," Opt. Lett., Vol. 24, No. 17, 1248-1250, 1999.

[31] A. V. Sokolov, D. D. Yavuz, D. R. Walker, G. Y. Yin, and S. E. Harris, "Light modulation at molecular frequencies," Phys. Rev. A, Vol. 63, 051801, 2001.

[32] A. V. Sokolov, D. R. Walker, D. D. Yavuz, G. Y. Yin, and S. E. Harris, "Raman Generation by Phased and Antiphased Molecular States," Phys. Rev. Lett, Vol. 85, No. 3, 562-565, 2000.

[33] A. V. Sokolov, D. R. Walker, D. D. Yavuz, G. Y. Yin, and S. E. Harris, "Femtosecond Light Source for Phase-Controlled Multiphoton Ionization," Phys. Rev. Lett., Vol. 87, No. 3, 033402, 2001.

[34] F. L. Kien, K. Hakuta, and A. V. Sokolov, "Pulse compression by parametric beating with a prepared Raman coherence," Physical Review A, 66, 023813, 2002.

[35] http://online.itp.ucsb.edu/online/qo02/sokolov

[36] http://online.itp.ucsb.edu/online/atto_c06/sokolov/

[37] http://www.photonics.com/Article.aspx?AID=40753

[38] http://www.optoiq.com/index/display/article-display/9916880149/articles/laser-focus-world/volume-46/issue-2/world-news/fiber-lasers__erbium-doped.html

[39] G. Krauss, T. Hanke, A. Sell, S. Eggert, R. Huber, and A. Leitenstorfer, "Single-cycle light pulses from a compact Er:fiber laser," OSA / CLEO / QELS, 1-2, May 2010.

[40] A. B. Shvartsburg, Time-Domain Optics of Ultrashort Waveforms, *Clarendon Press, Oxford,* 1996.

[41] A. B. Shvartsburg, Impulse Time-Domain Electromagnetics of Continuous Media, *Birkhauser Verlag*, *Boston*, 1999.

[42] A. B. Shvartsburg, "Single-cycle waveforms and non-periodic waves in dispersive media (exactly solvable models)," *Physics – Uspekhi*, Vol. 41, No. 1, 77-94, 1998.

[43] Z. Wang, Z. Zhang, Z.Xu, Q. Lin. Space-time profiles of an ultrashort pulsed Gaussian beam. IEEE Journal of Quantum Electronics, Vol. 33, No. 4, 1997.

[44] U. Parali, and D. R. Alexander, "Interaction of a single-cycle laser pulse with a bound electron without ionization," *Optics Express,* Vol. 18, No. 14, 15155-15168, July 2010.

[45] U. Parali, and D. R. Alexander, "Modeling the interaction of a single-cycle laser pulse with a bound electron without ionization," Book Chapter in *Coherence and Ultrashort Pulsed Emission* (in press), ISBN: 978-953-307-242-5, Intech Open Access Publisher, 2010.

[46] U. Parali, and D. R. Alexander, "Volterra integral equation solution of the convolutional modifier function approach for ultrashort single-cycle light pulse interaction with a bound electron without ionization," Submitted to Optics Express, November 2010.

[47] R. M. Joseph, S. C. Hagness, and A. Taflove, "Direct time integral of Maxwell's equations in linear dispersive media with absorption for scattering and propagation of femtosecond electromagnetic pulses," *Optics Letters*, Vol. 16, No. 18, September 15, 1991.

[48] S. L. Dvorak, and D. G. Dudley, "Propagation of ultra wideband electromagnetic pulses through dispersive media," IEEE Transaction of Electromagnetic Compatibility, Vol. 37. No. 2, May 1995.

[49] S. A. Kozlov, and S. V. Sazanov, "Nonlinear propagation of optical pulses of a few oscillations duration in dielectric media," *JETP* 84 (2), February 1997.

[50] H. Wilkelmsson, J. H. Trombert, J. F. Eloy. Dispersive and dissipative medium response to an ultrashort pulse: A green's function approach. *Physica Scripta*, Vol. 52, 102-107, 1995.

[51] P. Kinsler, and G. H. C. New, "Few-cycle pulse propagation," *Physical Review* A 67, 023813, 2003.

[52] J. F. Eloy, and F. Moriamez, "Spectral analysis of EM ultrashort pulses at coherence limit," Modelling, *SPIE Intense Microwave and Particle Beams III*, Vol. 1629, 1992.

[53] J. F. Eloy, and H. Wilhelmsson, "Response of a bounded plasma to ultrashort pulse excitation," *Physica Scripta*, Vol. 55, 475-477, 1997.

[54] M. Pietrzyk, I. Kanattsikov, and U. Bandelow, "On the propagation of vector ultrashort pulses," *Journal of Nonlinear Mathematical Physics*, Vol. 15, No. 2, 162-170, 2008.

[55] B. Macke, and B. Segard, "Propagation of light pulses at a negative group velocity," European *Physical Journal D*, Vol. 23, 125-141, 2003.

[56] Q. Zou, and B. Lu, "Propagation properties of ultrashort pulsed beams with constant waist width in free space," Optics and Laser Technology, Vol. 39, 619-625, 2007.

[57] H. Xiao, and K. E. Oughstun, "Failure of the group velocity description for ultrawideband pulse propagation in a casually dispersive, absorptive

dielectric," Journal of Optical Society of America B, Vol. 16, No. 10, October 1999.

[58] A. L. Gutman, "Electrodynamics of short pulses for pulse durations comparable to relaxation times of a medium," *Dokl. Physics*, Vol. 43, No. 6, 343-345, 1998.

[59] D. Hovhannisyan, "Propagation of a femtosecond laser pulse of a few optical oscillations in a uniaxial crystal," *Microwave and Optical Technology Letters*, Vol. 36, No. 4, February 2003.

[60] A. N. Berkovsky, S. A. Kozlov, and Y. A. Shpolyanskiy, "Self-focusing of few-cycle light pulses in dielectric media," Physical Review A, 72, 043821, 2005.

[61] A. Zewail, "Femtochemistry: atomic-scale dynamics of the chemical bond," *Journal of Physical Chemistry A*, Vol. 104, 5660–5694, 2000.

[62] M. A. Porras, "Nonsinusoidal few-cycle pulsed light beams in free space," *Journal of Optical Society of America B*, Vol. 16, No. 9, September 1999.

[63] V. G. Bespalov, S. A. Kozlov, Y. A. Shpolyanskiy, and I. A. Walmsley, "Simplified field wave equations for the nonlinear propagation of extremely short light pulses," Physical Review A, 66, 1-10, 2002.

[64] K. Akimoto, "Properties and Applications of ultrashort electromagnetic mono- and sub- cycle waves," *Journal of the Physical Society of Japan*, Vol. 65, No. 7, 2020-2032, 1996.

[65] X. Tan, X. Fan, Y. Yang, and D. Tong, "Time evolution of few-cycle pulse in a dense V-type three level medium," J. Modern Optics, Vol. 55, No. 15, 2439-2448, 2008.

[66] A. B. Shvartsburg, "Optics of nonstationary media," *Physics – Uspekhi*, Vol. 48, No. 8, 797-823, 2005.

[67] G. Steinmeyer, "A review of ultrafast optics and optoelectronics," J. Opt. A: Pure Appl. Opt. 5, R1-R15, 2003.

[68] J. E. Rothenberg, "Space-time focusing: Breakdown of the slowly varying envelope approximation in the self-focusing of femtosecond pulses," *Optics Letters*, Vol. 17, No. 19, October 1992.

[69] H. Kumagai, S. H. Cho, K. Ishikawa, K. Midorikawa, M. Fujimoto, S. Aoshima, and Y. Tsuchiya, "Observation of the comples propagation of a femtosecond laser pulse in a dispersive transparent bulk material," Journal of Optical Society of America, Vol. 20, No. 3, March 2003.

[70] M. D. Crisp, "Propagation of small-area pulses of coherent light through a resonant medium," Physical Review A, Vol. 1, No. 6, June 1970.

[71] B.K.P. Scaife. Principles of Dielectrics, Oxford University Press, Oxford, 1989.

[72] A. L. Gutman. Passage of short pulse throughout oscillating circuit with dielectric in condenser. Ultra-Wideband, Short-Pulse Electromagnetics 4, Kluwer Academic / Plenum Publishers, New York, 1999.

[73] V. V. Daniel. Dielectric Relaxation. Academic Press, New York, 1967.

[74] A. B. Shvartsburg, G. Petite. Progress in Optics, Vol. 44 (Ed. E Wolf), p. 143, Elsevier Sci, 2002.

[75] K. S. Cole, R. H. Cole. Dispersion and absorption in dielectrics. Journal of Chemical Physics, Vol. 9, 341-351, April 1941.

[76] A. B. Djurisic, E. H. Li. Modeling the index of refraction of insulating solids with a modified Lorentz oscillator model. *Applied Optics*, Vol. 37, No. 22, August 1998.

[77] E. Hecht, "Optics," 4th edition, Addison Wesley, 2002.

[78] R. W. Boyd, "Nonlinear Optics," Academic Press, Amsterdam, 2003.

[79] C. B. Schaffer. Interaction of femtosecond laser pulses with transparent materials, Ph.D. Thesis. Harvard University, May 2001.

[80] K. E. Oughstun, G. C. Sherman. Uniform asymptotic description of electromagnetic pulse propagation in a linear dispersive medium with absorption (the Lorentz medium). Journal of Optical Society of America A, Vol. 6, No. 9, 1394-1420, September 1989.

[81] L. N. Hand, J. D. Finch. Analytical Mechanics. Cambridge University Press, 7th edition, Cambridge, 2008.

[82] K. Maleknejad, and N. Aghazadeh, "Numerical solution of Volterra integral equations of the second kind with convolution kernel by using Taylor-series expansion method," *J. Appl. Math. Comput.* 161, 915-922, 2005.

[83] A. V. Kamyad, M. Mehrabinezhad, and J. S.Nadjafi, "A Numerical Approach for Solving Linear and Nonlinear Volterra Integral Equations with Controlled Error," *Int. J. App. Math.* 40 (2), May 2010.

[84] J. S. Nadjafi, and M. Heidari, "Solving linear integral equations of the second kind with repeated modified trapezoid quadrature method," *J. Appl. Math. Comput.* 189, 980-985, 2007.

[85] A. Adawi, and F. Awawdeh, "A Numerical Method for Solving Linear Integral Equations," *Int. J. Contemp. Math. Sciences,* Vol. 4, No. 10, 485-496, 2009.

[86] S. Yalcinbas, "Taylor polynomial solutions of nonlinear Volterra-Fredholm integral equations," *J. Appl. Math. Comput.* 127, 195-206, 2002.

[87] R. P. Kanwal, K. C. Liu, "A Taylor expansion approach for solving integral equations," *Int. J. Math. Educ. Sci. Technol.* 20 (3), 411, 1989.

[88] M. Sezer, "Taylor polynomial solution of Volterra integral equations," *Int. J. Math. Educ. Sci. Technol.* 25 (5), 625, 1994.

[89] S. A. Belbas, "On series solutions of Volterra equations," *J. Appl. Math. Comput.* 181, 1287-1304, 2006.

[90] N. A. Proite, B. E. Unks, J. T. Green, and D.D. Yavuz, "Refractive Index Enhancement with Vanishing Absorption in an Atomic Vapor, " *Physical Review Letters* 101(14), 147401(4), 2008.

[91] D.D. Yavuz, "Refractive Index Enhancement in a Far-Off Resonant Atomic System," *Physical Review Letters* 95(22), 223601(4), 2005.

[92] S. E. Harris, "Electromagnetically Induced Transparency," Physics Today, 36-42, July, 1997.

[93] S. E. Harris, "Refractive-index control with strong fileds," Opt. Lett., Vol. 19, No. 23, 2018-2020, 1994.

APPENDIX

A1. Matlab function for the solution of Laguerre USCP excitation with Modifier Function Approach

```
function f=modifierLagr
%%%%%%%%%%%%%%%%%%%%%%%%%%%%%%%%%%%%%%%%%%%%%%%%%%%%%%%%%%%%%%%%%%%%%%%%
% Written by Ufuk Parali
% Department of Electrical Engineering
% University of Nebraska, Lincoln, 2010
% This program calculates the outputs in Section 2.1 and 2.2 of this
% thesis for Laguerre USCP excitation with Modifier Function Approach.
%%%%%%%%%%%%%%%%%%%%%%%%%%%%%%%%%%%%%%%%%%%%%%%%%%%%%%%%%%%%%%%%%%%%%%%%
clear all
format long
gama=1e16;
spring=525;
mass=9.11e-31;
e=-1.6e-19;
z=5e-9;
c=3e8;
too=1e-15;
h=1e-18;
```

```
Eoo=0.65e3;
counter=1;
for t=0:h:8e-16
   FF5(counter)=-Eoo*exp(-((t-4e-16-z*c^-1)*7.5/(too))^2)*((-1/24)*((t-4e-16-z*c^-1)/too)^4+(15/24)*((t-4e-16-z*c^-1)/too)^3-(5/2)*((t-4e-16-z*c^-1)/too)^2+2*((t-4e-16-z*c^-1)/too));
   dFF5(counter)=-15*Eoo*(-15/2*t+3e-15+15/2*z/c)/too^2*exp(-(-15/2*t+3e-15+15/2*z/c)^2/too^2)*(-1/24*(t-4e-16-z/c)^4/too^4+5/8*(t-4e-16-z/c)^3/too^3-5/2*(t-4e-16-z/c)^2/too^2+2*(t-4e-16-z/c)/too)-Eoo*exp(-(-15/2*t+3e-15+15/2*z/c)^2/too^2)*(-1/6*(t-4e-16-z/c)^3/too^4+15/8*(t-4e-16-z/c)^2/too^3-5*(t-4e-16-z/c)/too^2+2/too);
   ddFF5(counter)=225/2*Eoo/too^2*exp(-(-15/2*t+3e-15+15/2*z/c)^2/too^2)*(-1/24*(t-4e-16-z/c)^4/too^4+5/8*(t-4e-16-z/c)^3/too^3-5/2*(t-4e-16-z/c)^2/too^2+2*(t-4e-16-z/c)/too)-225*Eoo*(-15/2*t+3e-15+15/2*z/c)^2/too^4*exp(-(-15/2*t+3e-15+15/2*z/c)^2/too^2)*(-1/24*(t-4e-16-z/c)^4/too^4+5/8*(t-4e-16-z/c)^3/too^3-5/2*(t-4e-16-z/c)^2/too^2+2*(t-4e-16-z/c)/too)-30*Eoo*(-15/2*t+3e-15+15/2*z/c)/too^2*exp(-(-15/2*t+3e-15+15/2*z/c)^2/too^2)*(-1/6*(t-4e-16-z/c)^3/too^4+15/8*(t-4e-16-z/c)^2/too^3-5*(t-4e-16-z/c)/too^2+2/too)-Eoo*exp(-(-15/2*t+3e-15+15/2*z/c)^2/too^2)*(-1/2*(t-4e-16-z/c)^2/too^4+15/4*(t-4e-16-z/c)/too^3-5/too^2);
   realtime(counter)=t;
   counter=counter+1;
end
```

```
dummy=size(realtime);
final=dummy(2);
for i=1:1:final
   P(i)=2*dFF5(i)+gama*FF5(i);
   Q(i)=ddFF5(i)+gama*dFF5(i)+(spring/mass)*FF5(i);
end
for i=1:1:final
   A(i)=(FF5(i)/h^2)+P(i)/(2*h);
   B(i)=Q(i)-2*FF5(i)/h^2;
   C(i)=(FF5(i)/h^2)-P(i)/(2*h);
   D(i)=(e/mass)*FF5(i);
end
for i=2:1:final
   M(i-1,i)=A(i-1);
end
for i=1:1:final
   M(i,i)=B(i);
end
for i=2:1:final
   M(i,i-1)=C(i);
end
Xto=0;
Xtf=0;
```

```
D(1)=D(1)-C(1)*Xto;
D(final)=D(final)-A(final)*Xtf;
D=D';
x=(M\D);
FF5=FF5';
totaleffect=FF5.*x;
D=D';
FF5=FF5';
for i=1:1:final
    P(i)=(1/FF5(i))*(2*dFF5(i)+gama*FF5(i));
    Q(i)=(1/FF5(i))*(ddFF5(i)+gama*dFF5(i)+(spring/mass)*FF5(i));
end
figure('Name','FF5'),plot(realtime,FF5),grid on,xlim([0 8e-16])
figure('Name','modifier'),plot(realtime,x),xlabel('t(sec)'),ylabel('ModifierFunction
(C.m/N)'),xlim([0 8e-16])
figure('Name','totaleffect'),plot(realtime,totaleffect),xlabel('t
(sec)'),ylabel('Oscillation Amplitude (m)');xlim([0 8e-16])
figure('Name','P'),plot(realtime,P),xlim([0 8e-16]),ylabel('Time varying damping
coefficient (Hz)'),xlabel('t (sec)'),axis([0 8e-16 -4e18 7e18])
figure('Name','Q'),plot(realtime,Q),grid on,xlim([0 8e-16]),ylabel('Time varying
spring coefficient (N/m)'),xlabel('t (sec)'),axis([0 8e-16 -1.5e34 2.5e34])
return;
```

A2. Matlab function for the solution of Hermitian USCP excitation with Modifier Function Approach

```
function f=modifierHerm
%%%%%%%%%%%%%%%%%%%%%%%%%%%%%%%%%%%%%%%%%%%%%%%%%%%%%%%%%%%%%%%%
% Written by Ufuk Parali
% Department of Electrical Engineering
% University of Nebraska, Lincoln, 2010
% This program calculates the outputs in Section 2.1 and 2.2 of this
% thesis for Hermitian USCP excitation with Modifier Function Approach.
%%%%%%%%%%%%%%%%%%%%%%%%%%%%%%%%%%%%%%%%%%%%%%%%%%%%%%%%%%%%%%%%
clear all
format long
gama=1e17;
spring=525;
mass=9.11e-31;
e=-1.6e-19;
z=5e-9;
c=3e8;
too=1e-15;
h=1e-16;
Eoo=1e2;
counter=1;
C=0.86733;
```

```
phi=4e-15;
for t=0:h:10*too
   FF5(counter)=Eoo*C*(1-((t-phi-z*c^-1)/too)^2)*exp(-(((t-phi-z*c^-1)/too)^2)/2);
   dFF5(counter)=-2*Eoo*C*(t-phi-z/c)/too^2*exp(-1/2*(t-phi-z/c)^2/too^2)-
Eoo*C*(1-(t-phi-z/c)^2/too^2)*(t-phi-z/c)/too^2*exp(-1/2*(t-phi-z/c)^2/too^2);
   ddFF5(counter)=-2*Eoo*C/too^2*exp(-1/2*(t-phi-z/c)^2/too^2)+4*Eoo*C*(t-phi-
z/c)^2/too^4*exp(-1/2*(t-phi-z/c)^2/too^2)-Eoo*C*(1-(t-phi-
z/c)^2/too^2)/too^2*exp(-1/2*(t-phi-z/c)^2/too^2)+Eoo*C*(1-(t-phi-z/c)^2/too^2)*(t-
phi-z/c)^2/too^4*exp(-1/2*(t-phi-z/c)^2/too^2);
   realtime(counter)=t;
   counter=counter+1;
end
dummy=size(realtime);
final=dummy(2);
for i=1:1:final
   P(i)=2*dFF5(i)+gama*FF5(i);
   Q(i)=ddFF5(i)+gama*dFF5(i)+(spring/mass)*FF5(i);
end
for i=1:1:final
   A(i)=(FF5(i)/h^2)+P(i)/(2*h);
   B(i)=Q(i)-2*FF5(i)/h^2;
   C(i)=(FF5(i)/h^2)-P(i)/(2*h);
   D(i)=(e/mass)*FF5(i);
```

```
end
for i=2:1:final
   M(i-1,i)=A(i-1);
end
for i=1:1:final
   M(i,i)=B(i);
end
for i=2:1:final
   M(i,i-1)=C(i);
end
Xto=0;
Xtf=0;
D(1)=D(1)-C(1)*Xto;
D(final)=D(final)-A(final)*Xtf;
D=D';
x=(M\D);
FF5=FF5';
totaleffect=FF5.*x;
nreal=real(sqrt(1+(avogadro*e*totaleffect)./(epsO*FF5)));
nimag=imag(sqrt(1+(avogadro*e*totaleffect)./(epsO*FF5)));
D=D';
FF5=FF5';
for i=1:1:final
```

```
    P(i)=(1/FF5(i))*(2*dFF5(i)+gama*FF5(i));
    Q(i)=(1/FF5(i))*(ddFF5(i)+gama*dFF5(i)+(spring/mass)*FF5(i));
end
figure('Name','FF5'),plot(realtime,FF5),grid on,title('Applied Ultrashort Single-Cycle
Hermitian Pulse');
figure('Name','modifier'),plot(realtime,x),xlabel('t (sec)'),ylabel('Dipole Moment per
Unit Force (C.m/N)');
figure('Name','totaleffect'),plot(realtime,totaleffect),xlabel('t(sec)'),ylabel('Oscillation
Amplitude (m)');
figure('Name','nreal'),plot(realtime,nreal),grid on
return;
```

A3. Matlab function for the solution of Laguerre USCP excitation with Concolutional Modifier Function Approach

```
function f=convModifierLagr
%%%%%%%%%%%%%%%%%%%%%%%%%%%%%%%%%%%%%%%%%%%%%%%%%%%%%%%%%%%%%%%%
% Written by Ufuk Parali
% Department of Electrical Engineering
% University of Nebraska, Lincoln, 2010
% This program calculates the outputs in Section 3.2 of this thesis for
% Laguerre USCP excitation with Convolutional Modifier Function Approach
%%%%%%%%%%%%%%%%%%%%%%%%%%%%%%%%%%%%%%%%%%%%%%%%%%%%%%%%%%%%%%%%
clear all
format long
gama=1e14;
spring=525;
mass=9.11e-31;
qe=-1.6e-19;
z=5e-9;
c=3e8;
epsO=8.854e-12;
avogadro=6.02e23;
too=1e-15;
h=1e-18;
Eo=0.65e3;
```

```
fo=1;
fnum=1;
timecounter1=1;
timecounter2=1;
for t=0:h:8e-16
   realtime(timecounter1)=t;
   timecounter1=timecounter1+1;
end
for t=0:h:16e-16
   realtimeconv(timecounter2)=t;
   timecounter2=timecounter2+1;
end
timesize=size(realtime);
final=timesize(2);
for i=1:1:final
   A(i)=(1/(h^2))+(gama/(2*h));
   B(i)=(spring/mass)-(2/(h^2));
   C(i)=(1/(h^2))-(gama/(2*h));
end
for i=2:1:final
   M(i-1,i)=A(i-1);
end
for i=1:1:final
```

```
   M(i,i)=B(i);
end
for i=2:1:final
   M(i,i-1)=C(i);
end
Xto=0;
Xtf=0;
x1convsum=zeros(1,2*final-1);
x2convsum=zeros(1,2*final-1);
for a=1:1:fnum
   counter=1;
   for t=0:h:8e-16
      if a==1
         E(counter)=-Eo*exp(-((t-4e-16-z*c^-1)*7.5/(too))^2)*((-1/24)*((t-4e-16-z*c^-
1)/too)^4+(15/24)*((t-4e-16-z*c^-1)/too)^3-(5/2)*((t-4e-16-z*c^-1)/too)^2+2*((t-4e-
16-z*c^-1)/too)); % Laguerre USCP
      end
      f1(counter)=fo*(exp(-((t-z*c^-1)/(too))^2)-sin((t-z*c^-1)/too)^(-a));
      f2(counter)=fo*(exp(-((t-z*c^-1)/(too))^2)+sin((t-z*c^-1)/too)^(-a));
      df1(counter)=fo*(- (2*t - (2*z)/c)/(too^2*exp((t - z/c)^2/too^2)) - (a*cos((t -
z/c)/too)*sin((t - z/c)/too)^(a - 1))/too);
```

```
        ddf1(counter)=fo*((2*t-(2*z)/c)^2/(too^4*exp((t-z/c)^2/too^2)) - 2/(too^2*exp((t
- z/c)^2/too^2)) + (a*sin((t - z/c)/too)*sin((t - z/c)/too)^(a - 1))/too^2 - (a*cos((t -
z/c)/too)^2*sin((t - z/c)/too)^(a - 2)*(a - 1))/too^2);
        df2(counter)=fo*((a*cos((t - z/c)/too)*sin((t - z/c)/too)^(a - 1))/too - (2*t -
(2*z)/c)/(too^2*exp((t - z/c)^2/too^2)));
        ddf2(counter)=fo*((2*t - (2*z)/c)^2/(too^4*exp((t - z/c)^2/too^2)) -
2/(too^2*exp((t - z/c)^2/too^2)) - (a*sin((t - z/c)/too)*sin((t - z/c)/too)^(a - 1))/too^2 +
(a*cos((t - z/c)/too)^2*sin((t - z/c)/too)^(a - 2)*(a - 1))/too^2);
        counter=counter+1;
    end
    F1=ddf1+gama*df1+(spring/mass)*f1-(qe/mass)*E;
    F1(1)=F1(1)-C(1)*Xto;
    F1(final)=F1(final)-A(final)*Xtf;
    F1=F1';
    xo1=(M\F1);
    x1conv(a,1:2*final-1)=h*conv(xo1,E);
    F2=ddf2+gama*df2+(spring/mass)*f2-(qe/mass)*E;
    F2(1)=F2(1)-C(1)*Xto;
    F2(final)=F2(final)-A(final)*Xtf;
    F2=F2';
    xo2=(M\F2);
    x2conv(a,1:2*final-1)=h*conv(xo2,E);
end
```

```
convsize=size(x1conv);
finalc=convsize(2);
for n=1:1:fnum
   x1convsum=x1convsum+x1conv(n,1:2*final-1);
   x2convsum=x2convsum+x2conv(n,1:2*final-1);
end
x1convfinal=x1convsum/fnum;
x2convfinal=x2convsum/fnum;
xconvfinal=(x1convfinal+x2convfinal)/2;
for n=1:1:final
   totaleffect(n)=xconvfinal(n);
end
nreal=real(sqrt(1+(avogadro*qe*totaleffect)./(epsO*E)));
nimag=imag(sqrt(1+(avogadro*qe*totaleffect)./(epsO*E)));
figure('Name','x1convfinal'),plot(x1convfinal),grid on;xlim([0 1600]);
figure('Name','x2convfinal'),plot(x2convfinal),grid on;xlim([0 1600]);
figure('Name','xconvfinal'),plot(realtimeconv,xconvfinal),grid on,xlim([0 16e-16]);
figure('Name','totaleffect'),plot(realtime,totaleffect),grid on,xlim([0 8e-16]);
figure('Name','nreal'),plot(realtime,nreal),grid on,xlim([0 8e-16]);
figure('Name','nimag'),plot(realtime,nimag),grid on,xlim([0 8e-16]);
return;
```

A4. Matlab function for the solution of Hermitian USCP excitation with Convolutional Modifier Function Approach

```
function f=convModifierHerm
%%%%%%%%%%%%%%%%%%%%%%%%%%%%%%%%%%%%%%%%%%%%%%%%%%%%%%%%%%%%%%%%%%%%%%%%
% Written by Ufuk Parali
% Department of Electrical Engineering
% University of Nebraska, Lincoln, 2010
% This program calculates the outputs in Section 3.2 of this thesis for
% Hermitian USCP excitation with Convolutional Modifier Function Approach
%%%%%%%%%%%%%%%%%%%%%%%%%%%%%%%%%%%%%%%%%%%%%%%%%%%%%%%%%%%%%%%%%%%%%%%%
clear all
format long
gama=1e14;
spring=4;
mass=9.11e-31;
qe=-1.6e-19;
z=5e-9;
c=3e8;
epsO=8.854e-12;
avogadro=6.02e23;
too=1e-15;
h=1e-16;
Eo=1e2;
```

```
fo=1;
fnum=1;
Const=0.86733;
phi1=4e-15;
timecounter1=1;
timecounter2=1;
for t=0:h:8e-15
   realtime(timecounter1)=t;
   timecounter1=timecounter1+1;
end
for t=0:h:16e-15
   realtimeconv(timecounter2)=t;
   timecounter2=timecounter2+1;
end
timesize=size(realtime);
final=timesize(2);
for i=1:1:final
   A(i)=(1/(h^2))+(gama/(2*h));
   B(i)=(spring/mass)-(2/(h^2));
   C(i)=(1/(h^2))-(gama/(2*h));
end
for i=2:1:final
   M(i-1,i)=A(i-1);
```

```
end
for i=1:1:final
   M(i,i)=B(i);
end
for i=2:1:final
   M(i,i-1)=C(i);
end
Xto=0;
Xtf=0;
x1convsum=zeros(1,2*final-1);
for a=1:1:fnum
   counter=1;
   for t=0:h:8e-15
      if a==1
         E(counter)=Eo*Const*(1-((t-phi1-z*c^-1)/too)^2)*exp(-(((t-phi1-z*c^-
1)/too)^2)/2); % Hermitian USCP
      end
      f1(counter)=fo*(1-((t-phi1-z*c^-1)/too)^(-a)); % Hermitian Trial Function
      df1(counter)=fo*((t-phi1-z/c)/too)^(-a)*a/(t-phi1-z/c); % Hermitian Trial
Function First Derivative
      ddf1(counter)=-fo*((t-phi1-z/c)/too)^(-a)*a^2/(t-phi1-z/c)^2-fo*((t-phi1-
z/c)/too)^(-a)*a/(t-phi1-z/c)^2; % Hermitian Trial Function Second Derivative
      counter=counter+1;
```

```
    end
    F1=ddf1+gama*df1+(spring/mass)*f1-(qe/mass)*E;
    F1(1)=F1(1)-C(1)*Xto;
    F1(final)=F1(final)-A(final)*Xtf;
    F1=F1';
    xo1=(M\F1);
    x1conv(a,1:2*final-1)=h*conv(xo1,E);
end
convsize=size(x1conv);
finalc=convsize(2);
for n=1:1:fnum
    x1convsum=x1convsum+x1conv(n,1:2*final-1);
end
x1convfinal=x1convsum/fnum;
for n=1:1:final
    totaleffect(n)=x1convfinal(n);
end
nreal=real(sqrt(1+(avogadro*qe*totaleffect)./(epsO*E)));
nimag=imag(sqrt(1+(avogadro*qe*totaleffect)./(epsO*E)));
figure('Name','totaleffect'),plot(realtime,totaleffect),grid on,xlim([0 8e-15]);
figure('Name','nreal'),plot(nreal),grid on;
figure('Name','nimag'),plot(nimag),grid on;
return;
```

A5. Matlab function for the solution of Laguerre USCP excitation with Convolutional Modifier Function Approach by solving VIE with modified Taylor Expansion Method

```
function f=convModifierVtrLagr
%%%%%%%%%%%%%%%%%%%%%%%%%%%%%%%%%%%%%%%%%%%%%%%%%%%%%%%%%%%%%%%%%%%%%%%%
% Written by Ufuk Parali
% Department of Electrical Engineering
% University of Nebraska, Lincoln, 2010
% This program calculates the outputs in Section 3.4 of this thesis for
% Laguerre USCP excitation with Convolutional Modifier Function Approach
% by solving Volterra Integral Equation with Modified Taylor Expansion Method
%%%%%%%%%%%%%%%%%%%%%%%%%%%%%%%%%%%%%%%%%%%%%%%%%%%%%%%%%%%%%%%%%%%%%%%%
clear all
format long
syms t tau to theta1 theta2 alpha beta a Eo fo Ett sprng gama mass charge
to=1e-15;
theta1=0.4167;
theta2=0.016667;
Eo=0.65e3;
fo=1;
Ett=-7.5293e-5;
alpha=((t-tau)/to)-theta1;
alphaf=(t/to)-theta1;
```

```
beta=(t/to)-theta2;

epsO=8.854e-12;

avogadro=6.02e23;

f1=fo*(exp(-beta^2)-sin(beta^a));

f2=fo*(exp(-beta^2)+sin(beta^a));

E=-Eo*exp(-(7.5*alpha)^2)*((-1/24)*alpha^4+(15/24)*alpha^3-
(5/2)*alpha^2+2*alpha);

Ef=-Eo*exp(-(7.5*alphaf)^2)*((-1/24)*alphaf^4+(15/24)*alphaf^3-
(5/2)*alphaf^2+2*alphaf);

integrand1=E;

integrand2=E*(tau-t);

integrand3=E*((tau-t)^2);

integrand4=diff(E,t);

integrand5=diff(E,t,2);

df1=diff(f1,t);

ddf1=diff(f1,t,2);

df2=diff(f2,t);

ddf2=diff(f2,t,2);

I1=int(integrand1,tau,0,t);

I2=int(integrand2,tau,0,t);

I3=int(integrand3,tau,0,t);

I4=int(integrand4,tau,0,t);

I5=int(integrand5,tau,0,t);
```

```
xo1=(f1-df1*I2-0.5*ddf1*I3+0.5*Ett*df1*I3)/(1+I1-
I2*(Ett+I4)+0.5*(Ett^2)*I3+0.5*Ett*I3*I4-0.5*I3*I5);
xo2=(f2-df2*I2-0.5*ddf2*I3+0.5*Ett*df2*I3)/(1+I1-
I2*(Ett+I4)+0.5*(Ett^2)*I3+0.5*Ett*I3*I4-0.5*I3*I5);
xo=0.5*(xo1+xo2);
F=diff(xo,t,2)+gama*diff(xo,t)+(sprng/mass)*xo;
S=F+(charge/mass)*Ef;
fnum=1;
h=1e-18;
realtime=(0:h:8e-16);
convtime=(0:h:16e-16);
sz=size(realtime);
final=sz(2);
sprng=4;
gama=1e14;
mass=9.11e-31;
charge=-1.6e-19;
for i=1:1:final
   A(i)=(1/(h^2))+(gama/(2*h));
   B(i)=(sprng/mass)-(2/(h^2));
   C(i)=(1/(h^2))-(gama/(2*h));
end
for i=2:1:final
```

```
    M(i-1,i)=A(i-1);
end
for i=1:1:final
    M(i,i)=B(i);
end
for i=2:1:final
    M(i,i-1)=C(i);
end
for a=1:1:fnum
    for i=1:1:final
        t=realtime(i);
        if (a==1)
            eval_Ef(i)=eval(Ef);
            eval_I1(i)=eval(I1);
            eval_I2(i)=eval(I2);
            eval_I3(i)=eval(I3);
            eval_I4(i)=eval(I4);
            eval_I5(i)=eval(I5);
        end
        eval_S(i)=eval(S);
    end
    if (a==1)
        eval_S=eval_S';
```

```
    end
    ft=M\eval_S;
    ft=ft';
    for k=1:1:final-2
        dft(k+1)=(ft(k+2)-ft(k))/(2*h);
        ddft(k+1)=(ft(k)-2*ft(k+1)+ft(k+2))/(h^2);
    end
    dft(1)=dft(2);
    ddft(1)=ddft(2);
    dft(final)=dft(final-1);
    ddft(final)=ddft(final-1);
    xoV=(ft-dft.*eval_I2+(Ett*dft*0.5-ddft*0.5-(Ett^2)*0.5).*eval_I3)./(1+eval_I1-
eval_I2.*(Ett+eval_I4)+0.5*Ett*eval_I3.*(eval_I4-eval_I5));
    xVconv(a,1:2*final-1)=h*conv(xoV,eval_Ef);
end
xVconvsum=zeros(1,2*final-1);
for n=1:1:fnum
    xVconvsum=xVconvsum+xVconv(n,1:2*final-1);
end
xVconvfinal=xVconvsum/fnum;
for i=1:1:final
    totaleffect(i)=xVconvfinal(i);
end
```

```
nreal=real(sqrt(1+(avogadro*charge*totaleffect)./(epsO*eval_Ef)));
nimag=imag(sqrt(1+(avogadro*charge*totaleffect)./(epsO*eval_Ef)));
figure,plot(convtime,xVconvfinal),grid on;
figure('Name','nreal'),plot(realtime,nreal),grid on,xlim([0 8e-16]);
figure('Name','nimag'),plot(realtime,nimag),grid on,xlim([0 8e-16]);
return;
```

A6. Matlab function for the solution of Hermitian USCP excitation with Convolutional Modifier Function Approach by solving VIE with modified Taylor Expansion Method

```
function f=convModifierVtrHerm
%%%%%%%%%%%%%%%%%%%%%%%%%%%%%%%%%%%%%%%%%%%%%%%%%%%%%%%%%%%%%%%%%%%%%%%
% Written by Ufuk Parali
% Department of Electrical Engineering
% University of Nebraska, Lincoln, 2010
% This program calculates the outputs in Section 3.4 of this thesis for
% Laguerre USCP excitation with Convolutional Modifier Function Approach
% by solving Volterra Integral Equation with Modified Taylor Expansion Method
%%%%%%%%%%%%%%%%%%%%%%%%%%%%%%%%%%%%%%%%%%%%%%%%%%%%%%%%%%%%%%%%%%%%%%%
clear all
format long
syms t tau to theta1 theta2 alpha beta a Eo fo Ett sprng gama mass charge
to=1e-15;
theta1=0.4167;
theta2=0.016667;
Eo=0.65e3;
fo=1;
Ett=-7.5293e-5;
alpha=((t-tau)/to)-theta1;
alphaf=(t/to)-theta1;
```

```
beta=(t/to)-theta2;

epsO=8.854e-12;

avogadro=6.02e23;

f1=fo*(exp(-beta^2)-sin(beta^a));

f2=fo*(exp(-beta^2)+sin(beta^a));

E=-Eo*exp(-(7.5*alpha)^2)*((-1/24)*alpha^4+(15/24)*alpha^3-
(5/2)*alpha^2+2*alpha);

Ef=-Eo*exp(-(7.5*alphaf)^2)*((-1/24)*alphaf^4+(15/24)*alphaf^3-
(5/2)*alphaf^2+2*alphaf);

integrand1=E;

integrand2=E*(tau-t);

integrand3=E*((tau-t)^2);

integrand4=diff(E,t);

integrand5=diff(E,t,2);

df1=diff(f1,t);

ddf1=diff(f1,t,2);

df2=diff(f2,t);

ddf2=diff(f2,t,2);

I1=int(integrand1,tau,0,t);

I2=int(integrand2,tau,0,t);

I3=int(integrand3,tau,0,t);

I4=int(integrand4,tau,0,t);

I5=int(integrand5,tau,0,t);
```

```
xo1=(f1-df1*I2-0.5*ddf1*I3+0.5*Ett*df1*I3)/(1+I1-
I2*(Ett+I4)+0.5*(Ett^2)*I3+0.5*Ett*I3*I4-0.5*I3*I5);
xo2=(f2-df2*I2-0.5*ddf2*I3+0.5*Ett*df2*I3)/(1+I1-
I2*(Ett+I4)+0.5*(Ett^2)*I3+0.5*Ett*I3*I4-0.5*I3*I5);
xo=0.5*(xo1+xo2);
F=diff(xo,t,2)+gama*diff(xo,t)+(sprng/mass)*xo;
S=F+(charge/mass)*Ef;
fnum=1;
h=1e-18;
realtime=(0:h:8e-16);
convtime=(0:h:16e-16);
sz=size(realtime);
final=sz(2);
sprng=4;
gama=1e14;
mass=9.11e-31;
charge=-1.6e-19;
for i=1:1:final
   A(i)=(1/(h^2))+(gama/(2*h));
   B(i)=(sprng/mass)-(2/(h^2));
   C(i)=(1/(h^2))-(gama/(2*h));
end
for i=2:1:final
```

```
    M(i-1,i)=A(i-1);
end
for i=1:1:final
    M(i,i)=B(i);
end
for i=2:1:final
    M(i,i-1)=C(i);
end
for a=1:1:fnum
    for i=1:1:final
        t=realtime(i);
        if (a==1)
            eval_Ef(i)=eval(Ef);
            eval_I1(i)=eval(I1);
            eval_I2(i)=eval(I2);
            eval_I3(i)=eval(I3);
            eval_I4(i)=eval(I4);
            eval_I5(i)=eval(I5);
        end
        eval_S(i)=eval(S);
    end
    if (a==1)
        eval_S=eval_S';
```

```
    end
    ft=M\eval_S;
    ft=ft';
    for k=1:1:final-2
        dft(k+1)=(ft(k+2)-ft(k))/(2*h);
        ddft(k+1)=(ft(k)-2*ft(k+1)+ft(k+2))/(h^2);
    end
    dft(1)=dft(2);
    ddft(1)=ddft(2);
    dft(final)=dft(final-1);
    ddft(final)=ddft(final-1);
    xoV=(ft-dft.*eval_I2+(Ett*dft*0.5-ddft*0.5-(Ett^2)*0.5).*eval_I3)./(1+eval_I1-
eval_I2.*(Ett+eval_I4)+0.5*Ett*eval_I3.*(eval_I4-eval_I5));
    xVconv(a,1:2*final-1)=h*conv(xoV,eval_Ef);
end
xVconvsum=zeros(1,2*final-1);
for n=1:1:fnum
    xVconvsum=xVconvsum+xVconv(n,1:2*final-1);
end
xVconvfinal=xVconvsum/fnum;
for i=1:1:final
    totaleffect(i)=xVconvfinal(i);
end
```

```
nreal=real(sqrt(1+(avogadro*charge*totaleffect)./(epsO*eval_Ef)));
nimag=imag(sqrt(1+(avogadro*charge*totaleffect)./(epsO*eval_Ef)));
figure,plot(convtime,xVconvfinal),grid on;
figure('Name','nreal'),plot(realtime,nreal),grid on,xlim([0 8e-16]);
figure('Name','nimag'),plot(realtime,nimag),grid on,xlim([0 8e-16]);
return;
```